AD-A046 317 PRINCETON UNIV N J DEPT OF AEROSPACE AND MECHANICAL--ETC F/G 20/4
THREE-DIMENSIONAL SHOCK WAVE TURBULENT BOUNDARY LAYER INTERACTI--ETC(U)
OCT 77 D S DOLLING, C D COSAD, S M BOGDONOFF N60921-76-C-0053

UNCLASSIFIED AMS-1354 NL

| OF |
AD
A046317

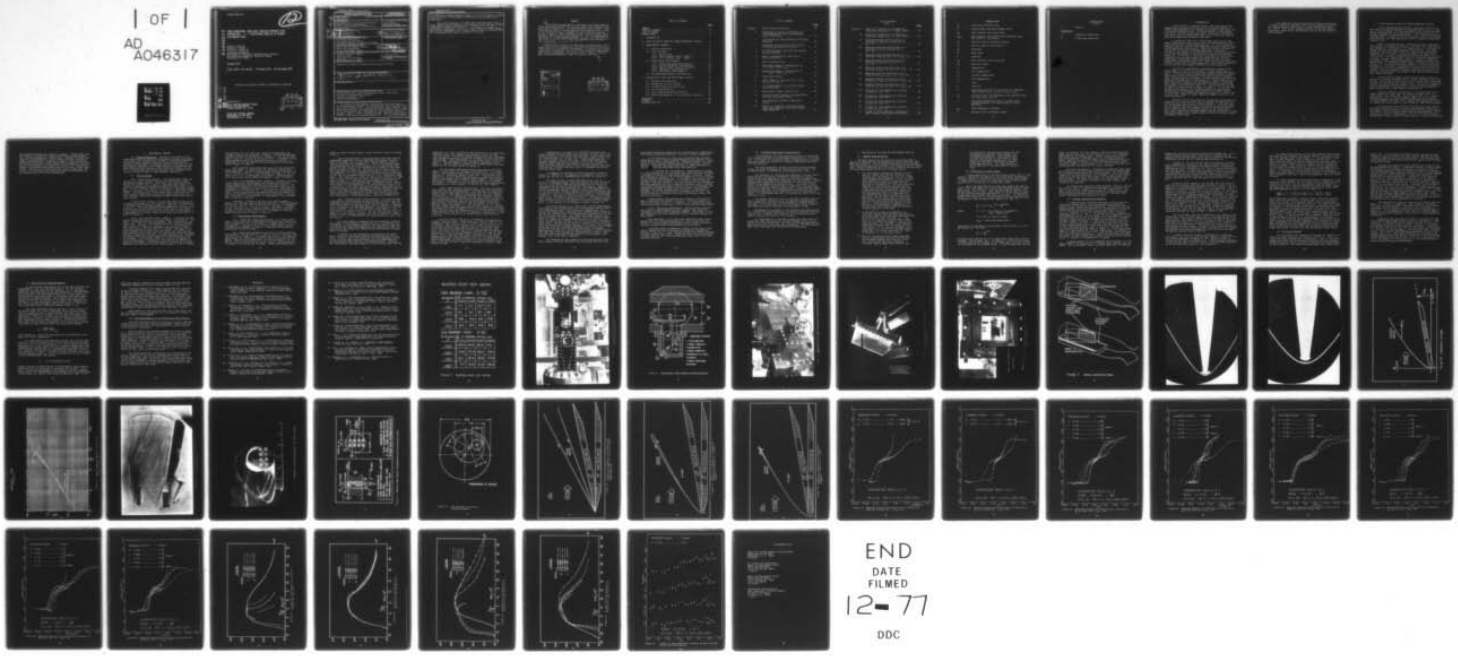

END
DATE
FILMED
12-77
DDC

REPORT AMS-1354

12

B-5.

AD A046317

THREE-DIMENSIONAL SHOCK WAVE TURBULENT BOUNDARY LAYER INTERACTIONS —— A PRELIMINARY ANALYSIS OF BLUNTED FIN-INDUCED FLOWS

David S. Dolling
Charles D. Cosad
Seymour M. Bogdonoff

PRINCETON UNIVERSITY
Department of Aerospace and Mechanical Sciences
Gas Dynamics Laboratory, Forrestal Campus
Princeton, NJ 08540

OCTOBER 1977

FINAL REPORT FOR PERIOD 1 OCTOBER 1975 - 30 SEPTEMBER 1977

Approved for public release; distribution unlimited

Prepared for

NAVAL SURFACE WEAPONS CENTER
WHITE OAK LABORATORY
SILVER SPRING, MD 20910

NAVAL AIR SYSTEMS COMMAND
DEPARTMENT OF THE NAVY
WASHINGTON, D.C. 20361

UNCLASSIFIED

SECURITY CLASSIFICATION OF THIS PAGE (When Data Entered)

REPORT DOCUMENTATION PAGE

READ INSTRUCTIONS BEFORE COMPLETING FORM

1. REPORT NUMBER: AMS-1354	2. GOVT ACCESSION NO.
3. RECIPIENT'S CATALOG NUMBER	
4. TITLE (and Subtitle): Three-Dimensional Shock Wave Turbulent Boundary Layer Interactions — A Preliminary Analysis of Blunted Fin-Induced Flows	5. TYPE OF REPORT & PERIOD COVERED: Final Report 10/1/75- 9/30/77
	6. PERFORMING ORG. REPORT NUMBER
7. AUTHOR(s): David S. Dolling, Charles D. Cosad, Seymour M. Bogdonoff	8. CONTRACT OR GRANT NUMBER(s): N60921-76-C-0053
9. PERFORMING ORGANIZATION NAME AND ADDRESS: Princeton University, Gas Dynamics Laboratory, Forrestal Campus, Princeton, NJ 08540	10. PROGRAM ELEMENT, PROJECT, TASK AREA & WORK UNIT NUMBERS
11. CONTROLLING OFFICE NAME AND ADDRESS: Naval Surface Weapons Center, White Oak Laboratory, Silver Spring, MD 20910	12. REPORT DATE: Oct [redacted] 77
	13. NUMBER OF PAGES: 59 (62 p.)
14. MONITORING AGENCY NAME & ADDRESS (if different from Controlling Office): Naval Air Systems Command, Code AIR-320C, Department of the Navy, Washington, D. C. 20361	15. SECURITY CLASS. (of this report): Unclassified
	15a. DECLASSIFICATION/DOWNGRADING SCHEDULE

16. DISTRIBUTION STATEMENT (of this Report)

Approved for public release; distribution unlimited

17. DISTRIBUTION STATEMENT (of the abstract entered in Block 20, if different from Report)

Final rept. 1 Oct 75- 30 Sep 77,

18. SUPPLEMENTARY NOTES

19. KEY WORDS (Continue on reverse side if necessary and identify by block number)

Three-dimensional shock wave-boundary layer interaction
Blunted fin-induced interaction
Turbulent boundary layer
Surface measurements

20. ABSTRACT (Continue on reverse side if necessary and identify by block number)

An extensive experimental investigation has been made of three-dimensional blunted fin-induced shock wave turbulent boundary layer interactions. Surface pressures, heat transfer rate distributions and oil streak patterns were obtained over a range of fin bluntnesses and incidences for two different incoming boundary layers. These incoming boundary layers had mean thicknesses in the ratio of approximately 4:1. All the measurements

DD FORM 1 JAN 73 1473 EDITION OF 1 NOV 65 IS OBSOLETE

UNCLASSIFIED

SECURITY CLASSIFICATION OF THIS PAGE (When Data Entered)

288 475

were made at a freestream Mach number of 3, a unit Reynolds number of 6.2×10^7 m^{-1} (1.6×10^6 in^{-1}) and with near adiabatic wall conditions.

Preliminary analysis of these data indicates that, over a large region of the interaction, the property distributions collapse using purely geometric parameters. In contrast to its two-dimensional counterpart, which is a highly Reynolds number dependent viscous phenomenon, the present results seem to indicate that the three-dimensional case is primarily inviscid.

SUMMARY

An extensive experimental investigation has been made of three-dimensional blunted fin-induced shock wave turbulent boundary layer interactions. Surface pressures, heat transfer rate distributions and oil streak patterns were obtained over a range of fin bluntnesses and incidences for two different incoming boundary layers. These incoming boundary layers had mean thicknesses in the ratio of approximately 4:1. All the measurements were made at a freestream Mach number of 3, a unit Reynolds number of 6.2×10^7 m^{-1} (1.6×10^6 in^{-1}) and with near adiabatic wall conditions.

Preliminary analysis of these data indicates that, over a large region of the interaction, the property distributions collapse using purely geometric parameters. In contrast to its two-dimensional counterpart, which is a highly Reynolds number dependent viscous phenomenon, the present results seem to indicate that the three-dimensional case is primarily inviscid.

TABLE OF CONTENTS

LIST OF FIGURES

LIST OF FIGURES
(cont)

NOMENCLATURE

A_s	slug cross-sectional area
D	leading edge bluntness diameter (DIA)
C_H	heat transfer rate coefficient
$C_{H_{vD}}$	heat transfer rate coefficient evaluated using van Driest II correlation
Cp	specific heat at constant pressure
C_s	specific heat of slug material
m_s	slug mass
M	Mach number
P	pressure
$\dot{q}_w$	heat transfer rate at the wall
Re	Reynolds number
T	temperature
T_w	wall temperature
T_r	recovery temperature
T_s	slug temperature
t	time
U	velocity
X	coordinate parallel to the tunnel axis measured from furthest point forward of shock wave
X_s	distance along instrumentation line measured from the shock wave location
Y	coordinate normal to X axis in plane of test surface measured from leading edge of shock generator
α_G	shock generator incidence
δ	boundary layer thickness (DELTA)

NOMENCLATURE
(cont)

ρ	density

Subscripts

o	stagnation conditions
∞	freestream conditions

1. INTRODUCTION

A vast amount of research effort, both experimental and theoretical, has been and continues to be aimed at gaining a better understanding of the interaction between a shock wave and a turbulent boundary layer. Of these studies, a large proportion have involved the two-dimensional interaction, typified by that occurring on a compression ramp or on a plane wall with an externally generated impinging shock wave.

In practice, nearly all interactions occurring on high speed flight vehicles are either fully three-dimensional or display some degree of three-dimensionality. It is only recently, however, that any detailed investigations have been made of these three-dimensional interactions. These are briefly discussed in the review of previous investigations given in Section 2. Primarily, the neglect of three-dimensional interactions has been due to the experimental difficulties of resolving the complex flowfield. It is also in part due to the desire to have understood and have developed prediction techniques for the two-dimensional interaction, before attempting to model the more complicated three-dimensional flow. Very few of these interaction studies, either two- or three-dimensional, have been carried out at the high Reynolds numbers typical of flight conditions.

The current experimental investigation, planned as the first stage of a continuing program, is a major extension of earlier work carried out using a sharp leading edged shock generator. In this new study, an extensive parametric study of three-dimensional blunted fin-induced shock wave turbulent boundary layer interactions has been made. Surface property distributions have been measured over a wide range of fin bluntnesses and incidences for two different incoming boundary layers. These boundary layers were generated on two model configurations and had thicknesses in the ratio of about 4:1. The test matrix covered for both of these studies is shown in Figure 1. All of the measurements were made in the Princeton University Gas Dynamics Laboratory's high Reynolds number supersonic blowdown tunnel. In this tunnel, unit Reynolds numbers as high as 3×10^8 m^{-1} can be generated. Based on length, Reynolds numbers close to 1 billion are possible.

The main aim in this study was to make the surface measurements and to incorporate them into a computerized data bank, in a form suitable for a future in-depth analysis. From the large and unique data bank built up in this study, it should be possible to identify the key parameters controlling the surface property distributions in different regions of the interaction. This report describes the experimental program carried out to make these measurements and presents details of the preliminary analysis made on these data.

This research project was carried out during the period 1 October 1975 to 30 September 1977 and was funded by the Naval Air Systems Command under contract number N60921-76-C-0053. Dr. Irwin E. Vas, Senior Research Engineer at the Gas Dynamics Laboratory, made a major contribution during the test phase of this program.

2. BRIEF REVIEW OF PREVIOUS THREE-DIMENSIONAL STUDIES

In the three-dimensional domain, the state of the art is not very far advanced compared to two-dimensional flows. A number of studies (Refs. 1-6) has been made of the three-dimensional flowfields generated by protuberances, either partially or completely immersed in the boundary layer. Such investigations have provided useful information on the interaction scale, the surface flow patterns, and some qualitative data on regions of high heat transfer rate.

Other investigations have examined particular aspects of the blunted fin-induced interaction. Price and Stallings (Ref.7) laid emphasis on the effect of fin sweep angle, fin thickness and height upon the interaction pressure distribution. The shock generator used had a hemicylindrical leading edge and was maintained at zero incidence. Tests were made in the Mach number range 2.3 to 4.4 and at freestream unit Reynolds numbers up to 15×10^6 m^{-1}. Gillerlain (Refs. 8,9) has used phase change paints to study fin-body interference heating on a cone-fin model and also made limited pressure measurements. Kaufmann, Korkegi and Morton (Ref. 10) obtained surface pressure distributions and pitot profiles in the interaction region ahead of a hemi-cylindrically blunted fin. Schlieren photographs from this study showed the interaction flow to be unsteady but no quantitative data were obtained. These measurements suggested that the amplitude of the oscillation was several times greater than the undisturbed boundary layer thickness.

Studies such as these, as well as many others, have resulted in a greater understanding of certain aspects of the interaction. This is particularly true in the region around and ahead of the fin nose and on the latter itself. As far as is known, no studies have been extensive enough in their variation of geometric and flow parameters to successfully determine those parameters which control the surface property distributions.

Up until recently, the majority of the data available on these interactions came from the studies of McCabe (Ref. 11), Lowrie (Ref. 12), Token (Ref. 13) and Peake (Ref. 14). These investigations, all in the Mach number range 2 to 4, involved a shock wave emanating from a sharp leading edged shock generator. In these studies, the area of the interaction examined was limited in extent and little detail of the flowfield itself was provided.

A considerably more extensive and detailed study, carried out under contract to the Air Force Flight Dynamics Laboratory, was made at the Gas Dynamics Laboratory during the period 1973-75. This study, also involving a sharp leading edged generator, is reported on in detail in References 15 to 17. In a well defined experimental set-up, detailed surface and full flowfield properties

were measured through the interaction region. Surface data from this study illustrated the sharply contrasting trends between two- and three-dimensional interactions. Upstream influence was shown to be independent of shock strength with the interaction length decreasing with increasing incidence. More importantly, the detailed flowfield surveys showed the flow ahead of the shock wave to be dominated by an extensive inviscid flow interference between the upstream compression waves and the main oblique shock itself. Data from this study have been used by Hayes (Ref. 18) as part of a data base for developing prediction techniques for the characteristics of these interactions.

3. EXPERIMENTAL PROGRAM

3.1 General Objectives. The aim at the start of this investigation was to conduct an experimental program which would yield sufficient relevant data to identify those key parameters controlling the interaction surface property distributions. Extensive use was made of equipment developed previously at the Gas Dynamics Laboratory for investigations of three-dimensional shock wave-turbulent boundary layer interactions (Refs. 15, 16, 17). A large proportion of this equipment was developed under contract to the Air Force Flight Dynamics Laboratory.

3.2 Test Equipment.

3.2.1 Wind tunnel facility. The experimental study was carried out in the Princeton University high Reynolds number supersonic blowdown tunnel. This tunnel has a working section 20 cm x 20 cm (8" x 8"), a nominal freestream Mach number of 3 and may be operated at stagnation pressures ranging from 4×10^5 Nm^{-2} to 34×10^5 Nm^{-2} (60 psia to 500 psia). The total temperature of the flow is typically in the range of 250°K-270°K (450°R-485°R). The actual value at any given time is determined by the local outside temperature, the Joule-Thompson drop across the main regulator valve and the amount of heat transferred from the inlet piping.

In the current study, all of the tests were carried out at a stagnation pressure of 6.8×10^5 Nm^{-2} (100 psia) corresponding to a freestream unit Reynolds number of about 6.3×10^7 m^{-1} (1.6×10^6 in^{-1}). With the above mentioned temperature considerations the model was at near adiabatic wall conditions for all tests. A full description of this facility can be found in Reference 17. A photograph of the tunnel showing the nozzle and test section is given in Figure 2.

3.2.2 Thick boundary layer - Model 1. Two model configurations formed the basis of this experimental investigation. The Model 1 configuration used the boundary layer developing on the tunnel wall. This is a two-dimensional fully turbulent boundary layer with a thickness $\delta \simeq 1.27$ cm ($\simeq .5$ in) in the region of the interaction. The shock generator used spanned the tunnel vertically and was 25.4 cm (10 in) in length. The edges of the shock generator which mated with the tunnel floor and ceiling were provided with a nylon seal to eliminate any leaks and reduce marring of contacted surfaces. The shock generator was supported by bearings near the leading edge and an arm extending in from the sidewall. This arm was linked to a screw drive mechanism which allowed manual adjustment of the angle of incidence by an external drive wheel. Since the center of rotation of the shock generator was displaced from the leading edge by a small distance,

the value of Y/δ or Y/D for a given instrumentation row changed slightly with generator incidence. This change was small and had no effect on the analysis. Values of Y/D in the test matrix (figure 1) are for an incidence of 0°. A schematic of the shock generator and drive mechanism is shown in Figure 3. A photograph of the test section and shock generator drive mechanism is shown in Figure 4.

Four different bluntnesses were used with the thick boundary layer (Model 1) study as well as the sharp leading edge shock generator. The blunt leading edges measured .318 cm (.125 in) to 1.27 cm (.500 in). This resulted in a range of D/δ of about .25 to 1.0. A photograph of the Model 1 shock generator with the various leading edge bluntnesses is shown in Figure 5.

3.2.3 Thin boundary layer - Model 2. The Model 2 configuration made use of the boundary layer developing on a sharp leading edged plate which spanned the tunnel horizontally. The incoming two-dimensional fully turbulent boundary layer had developed over a distance of about 30 cm ($\approx$ 12 in) resulting in a thickness $\delta \simeq .38$ cm (.15 in) in the region of the interaction start. The shock generator was mounted vertically between the plate and the tunnel ceiling and held and controlled in the same way as the Model 1 configuration. A photograph of this arrangement is shown in Figure 6.

Like Model 1, Model 2 had four blunt leading edges in addition to the sharp leading edge configuration. The bluntnesses varied from .102 cm (.040 in) to .406 cm (.160 in) in increments of .102 cm (.040 in). In a similar way to the Model 1 configuration using the thick incoming boundary layer, this resulted in a range of D/δ of about .25 to 1.0. A schematic of the two model configurations is shown in Figure 7.

3.3 Experimental Measurements.

3.3.1 Shock wave shape determination. Of primary importance in this study was a knowledge of the shock wave location at each incidence for all of the blunt tip diameters used in the investigation. To achieve this, a series of dummy models was constructed which spanned the range of incidences and bluntnesses encountered during the study.

Four leading edge diameters were used for these aluminum dummy models; .102 cm (.040 in), .318 cm (.125 in), .635 cm (.250 in) and 1.27 cm (.500 in). To include the effect of incidence on shock shape, four models were made for each of the above tip diameters. Each of these maintained a 12° included angle, i.e. 0° and 12°, 2° and 10°, 4° and 8°, and 6° and 6°. This allowed two incidences to be covered by one model. Shadow photographs were

taken for each of these models, two of which are shown in Figures 8 and 9.

The X-Y coordinates of the shock waves were read from the shadowgraph negatives using a Kodak Model 2A Contour Projector. With a ten power lens in place this offered excellent spatial resolution as well as repeatability. The X-Y coordinate system just mentioned has the X axis parallel to the undisturbed free-stream and the origin at the farthest point forward of the shock wave, as shown in Figure 10. The resulting X-Y coordinates of the shock wave were then non-dimensionalized by their respective tip diameters, D. For each angle of incidence the data from each of the four tip diameters were plotted on fully logarithmic graph paper. This resulted in a total of seven plots of (X/D) vs. (Y/D). Two of these, the 0° and 10° cases, are shown on the same set of axes in Figure 11. Knowledge of the stand-off distance of the shock wave from the nose was necessary to determine shock location with respect to instrumentation. For consistency a value of 0.3 x D was used. This figure was obtained from a compilation of an extensive amount of data presented by Liepmann and Roshko (Ref.19). Use of this technique for the assessment of the stand-off distance introduces no significant errors into the data analysis. An explanation of the method of use of these shock shape curves and a discussion of their application is given in Section 4.2.

3.3.2 Surface pressure distributions. For both the Model 1 and Model 2 configurations surface pressure distributions were measured along four different streamwise tapping rows. Each row consisted of about 50 tapping holes (.102 cm (.040in) in diameter) in a line parallel to the shock generator surface when it was set at 0° incidence. For the thick boundary layer (Model 1) case these were at Y values of 2.29 cm (.9 in), 4.83 cm (1.9 in), 7.37 cm (2.9 in) and 9.91 cm (3.9 in). For the thin boundary layer (Model 2) case, pressure tapping rows were situated at Y values of 2.92 cm (1.15 in), 5.46 cm (2.15 in), 8.64 cm (3.4 in) and 11.18 cm (4.4 in).

The large number of pressure taps was necessary to ensure the capture of the complete interaction for all bluntnesses and incidences. A considerable length of the test section required instrumentation, since the shock shape and location and hence the position of the interaction region varied considerably with generator bluntness.

The extent of the interaction downstream of the shock which is free of interference effects is determined by two factors. Firstly, the finite length of the shock generator results in the trailing edge expansion restricting the downstream distance available free from this interference effect. Secondly, for interference free measurements in the direction away from the

generator (i.e. the Y direction), the reflection of the shock wave from the tunnel wall opposite the generator surface is the limiting factor. The latter becomes progressively more important with increasing generator angles of incidence for any given blunt leading edge. This interference can be clearly seen in the surface oil flow photograph of the interaction generated by the Model 1, .635 cm (.250 in) diameter blunt leading edge shock generator at 10° incidence shown in Figure 12.

For both model configurations, surface pressure data were taken at seven angles of incidence, 0° through 12° in 2° increments. The maximum incidence was limited by tunnel stall which occurred at a generator angle of about 13°. The pressures were sampled by a 48 port Model 48J4 Scanivalve in conjunction with a Druck strain gauge type transducer (Model PDCR22). The pressure tappings were scanned at a rate of approximately 3.75 readings per second. The output of this transducer was then digitized and processed by an I.B.M. System 7 on line to an I.B.M. 360-91.

3.3.3 Heat transfer distributions. The local convective heat transfer rate was experimentally determined using the quasi-transient slug calorimeter method. The time rate of change of a copper slug of known physical properties gave the heat transfer rate directly. This method was selected for three main reasons. It could be easily incorporated into the test section in use, it gave acceptable spatial resolution and had been used successfully in previous experimental work at the Gas Dynamics Laboratory. Heat transfer rate distributions were determined for the thick boundary layer case (Model 1). This was carried out for each of the five leading edge configurations at seven angles of incidence, 0° through 12° in 2° increments (as in the surface pressure study). These distributions were measured along four rows parallel to the shock generator (when set at 0° incidence) at distances of 4.19 cm (1.65 in), 5.46 cm (2.15 in), 9.27 cm (3.65 in) and 10.54 cm (4.15 in).

For this study, a 5.08 cm (2 in) diameter plug containing 8 copper slugs was used. These slugs were .224 cm (.088 in) in diameter and were .051 cm (.020 in) thick, giving a mass of 17.8 milligrams. Each copper slug was held in place in the plug by a linen based phenolic ring .635 cm (.250 in) in diameter, thus minimizing any heat conduction between the slug and the brass plug. Two holes .015 cm (.006 in) in diameter were drilled near the center of the slug to accommodate two .013 cm (.005 in) diameter wires to form a Chromel-Alumel thermocouple. The thermocouple junction was then soldered to the slug. Chromel-Alumel thermocouples were installed symmetrically in the surface of the brass plug between the rows of slugs, since the procedure to be used in the data analysis required a knowledge of the wall temperature history.

Compressed air at about 8.3×10^5 Nm^{-2} (120 psia) was passed through a boiling water heat exchanger and then fed to the plug to serve as a heat source for the slugs. A small tube with an inside diameter of .102 cm (.040 in) was located .305 cm (.12 in) from the rear face of each slug. These eight tubes were brought together and fed by a single 1.27 cm (.50 in) diameter tube which was externally connected to the hot air supply. A three way hand operated valve in the line just ahead of the plug could be set to either heat the slugs or to exhaust the hot air into the tunnel room.

A photograph of the heat transfer plug used is shown in Figure 13. Details of the geometric arrangement of the calorimeters and the two wall thermocouples are given in Figure 14.

The heat transfer plug was designed to fit into an eccentric rotatable system. The test section features two 30.48 cm (12.0 in) diameter observation/instrumentation ports which face each other on the top and bottom tunnel walls. These are independent of the shock generator and its actuating mechanism and can accommodate optical windows, surface instrumentation, (as in the case of heat transfer studies), and probe drive mechanisms (as would be used in an extension of this study to flowfield measurements). The upper of the two ports can be seen in the photograph of the test section shown in Figure 4. The eccentric rotatable system allows the heat transfer plug to be located anywhere within a 20.3 cm (8.0 in) diameter circle flush with the tunnel wall. A line drawing of this system is shown in Figure 15.

The actual procedure for taking heat transfer measurements consisted of starting the tunnel and allowing the slugs to remain at a temperature close to the tunnel wall temperature. With steady flow established, the shock wave generator would be set at the desired incidence and the three-way valve opened to allow the hot air to heat the slugs. The slugs were heated typically to about 30°C above the wall temperature. With the constant temperature air supply, the overheat obtainable was a function of the local convective heat transfer rate in the particular interaction under study. The heating jet would then be cut off and the high speed data acquisition system started. After about 3 to 7 seconds the slugs would have reached a temperature well below that of the tunnel wall and the data recording system would be stopped. Readings were taken at a rate of 200 per second. With 10 channels, this resulted in 20 readings per thermocouple per second. The data were then digitized and processed via the in-house I.B.M. System 7 and I.B.M. 360-91 computers.

The temperature-time gradient of the slug from which the heat transfer rate was calculated was determined when the slug

calorimeter temperature equalled the surrounding wall temperature. This minimized non-uniformities in the test surface temperature.

A full discussion of this quasi-transient heat transfer technique as used at the Princeton University Gas Dynamics Laboratory can be found in Reference 20. Presented therein is a brief review of heat transfer methods used at the laboratory, and for the quasi-transient technique specifically, model construction, test procedures and data acquisition and reduction.

3.3.4 Surface oil flow patterns. Photographs of surface oil flow patterns for each bluntness were taken for both the Model 1 and Model 2 studies at each shock generator incidence. These were obtained by using a low viscosity commercial oil as a vehicle for a powdered fluorescent dye. If necessary, this mixture could be made thinner with kerosene. A thin coat of the mixture was applied to the test surface. The tunnel would then be started and the shock generator set at the desired incidence. Once a steady flow pattern was established, usually after 10 to 20 seconds, the photograph was taken through an optical window with the tunnel running. The streak patterns were recorded on 35mm Kodak Panatomic-X film in conjunction with a Wratten 2B filter. The filter served to eliminate ultra-violet reflections coming from the metal surfaces.

These surface flow patterns were reduced to quantitative data by measuring the angles of local oil lines with respect to the X axis along a line of Y = constant. For consistency, the Y values chosen were those used in the surface pressure measurements.

3.3.5 Additional measurements. During surface pressure distributions, measurements of total pressure were taken by a transducer located in the stagnation chamber. The output of this was recorded by the data system each time a pressure tapping row was scanned.

Both the Model 1 and 2 shock wave generators were instrumented with four surface pressure taps. One of these was connected to its own pressure transducer and the output recorded by the data system during surface pressure distributions.

A Chromel-Alumel thermocouple located in the tunnel stagnation chamber was used to monitor the stagnation temperature history of the flow. It was recorded during both surface pressure and heat transfer rate tests. These data were used quantitatively in calculation of the freestream Reynolds number and in the heat transfer analysis.

3.4 Estimated Measurement Uncertainties

The shadowgraph technique employed allowed for determination of shock location to an estimated accuracy of $\pm$ .13 cm (.05 in). This length is of the same order of magnitude as a pressure tapping diameter and therefore introduces effectively no error into the analysis.

The shock generator incidence calibration was obtained using a sine bar referenced to the opposite tunnel wall. The deflection angle is considered to be accurate to $\pm$ .05°.

All pressures in the study were measured by either Pace or Druck variable reluctance transducers referenced to vacuum. Calibrations were made before each run and were observed to be highly linear and repeatable throughout the test program. Surface pressures were measured via Scanivalves at a rate for which no errors from pressure-time lag would occur. The overall uncertainty of the static pressure data is estimated to be less than $\pm$ 2% of the upstream static pressure level. The stagnation chamber pressure during a run was maintained accurately by the tunnel operator by observing a null meter set to zero at the desired level. It is estimated that this is accurate to within 1% of the operation value.

The largest source of error in the heat transfer rates results from basic inaccuracies of the temperature measurements. This becomes more critical in the subsequent differentiation of the data. It is concluded that the final heat transfer data in the interaction has an accuracy of approximately $\pm$ 15%.

Photographs of surface oil flow patterns were obtained for all interactions investigated and the angles from these are accurate to $\pm$ 2°. However, the nature of this technique provides greater accuracy at higher oil flow angles.

All measurements in the test program were made under the assumption that flow variables remained "steady" at any fixed point within the interaction. No time resolved measurements were made to confirm or invalidate this assumption. Of these measurements made, none gave any indication of unsteadiness.

4. DISCUSSION OF THE DATA AND PRELIMINARY ANALYSIS

4.1 General Considerations

The major portion of the contract period was spent in making the experimental measurements and establishing the data bank now available. Only a preliminary analysis has been made. This exploratory work has focussed on the pressure and oil streak data. Before presenting any of the data, three points pertinent to these measurements are briefly discussed below.

1) The experimental program was designed around use of a tunnel test section originally constructed and instrumented for use with a sharp leading edged shock generator. Use of blunted shock generators resulted in the interaction start occurring further upstream than the available instrumentation. This was completely remedied for the pressure distributions by replacing a section of the tunnel floor with a new pressure plate designed to capture the interaction start under all test conditions. For photographing the oil streak patterns and installing the heat transfer rate instrumentation, both of which used the available ceiling port, the problem could not be overcome without major modifications to the test section. These restrictions imposed on some phases of the experimental program by using the available test section have not seriously hindered analysis of the data.

2) In the analysis, data are presented in a coordinate system where distance relative to the shock location has been non-dimensionalized by the boundary layer thickness δ. The value of δ used for any given case is the local value immediately ahead of the initial pressure rise. For the Model 1 configuration, these were obtained from the tunnel calibration tables. In the case of the Model 2 configuration, a series of pitot surveys made by Oskam (Ref. 15) on the same plate was used to determine δ at any given point.

3) Early in the data analysis, both sharp and blunted leading edge pressure distributions were plotted together as a function of X_s (i.e. relative to the shock location). The sharp leading edged shock location was

calculated from oblique shock theory and the blunted shock locations were obtained from the shadow photographs. These comparisons of sharp and blunted fin data made it clear that for consistency and accuracy the shock shapes for the sharp case should be determined experimentally. This measurement will be carried out in the next phase of the program.

4.2 Discussion of Shock Shapes

A close examination of the shock shape curves, X/D vs. Y/D, reveals interesting information on the shock waves encountered in the test program. The motivation for plotting the shock shapes in these coordinates on fully logarithmic scales came from the possibility of an analogy with blast-wave theory.

One of the applications of blast wave theory has been to predict the shock shape for a blunt leading edged plate in hypersonic flow. An analysis of this type was made by Baradell and Bertram (Ref. 21) in 1960. Their analysis showed that the shape of the detached shock was dominated by D for a distance downstream many times greater than the tip diameter. To predict the shape of the shock in this region Baradell and Bertram developed an equation of the following form (Equation 3, Ref. 21).

$$\frac{Y}{D} = f(n,\gamma)\, C_{D,n}^{\,1/3+n} \left(\frac{X}{D}\right)^{2/3+n}$$

where: $n = 0$ or 1 for planar or axisymmetric case, respectively

γ — ratio of specific heats

$C_{D,n}$ — nose drag coefficient

Application of the above to the current study results in a proportionality of the form:

$$\frac{Y}{D} \alpha \left(\frac{X}{D}\right)^{2/3}$$

A plot of this equation on fully logarithmic paper would yield a straight line of slope $2/3$. In Figure 11 a line of this slope is shown plotted as a tangent to the shock shape curves of 0° and 10° incidence for the present study. It can be seen that the $2/3$

power law relation for shock shape as developed from blast-wave theory applies very well to the region of 2 to 10 tip diameters downstream of the leading edge. Further downstream than this the shock generator incidence starts to influence the shock shape. Before this point the shock shape is determined only by the leading edge bluntness. As X/D increases, the shock shape curves of Figure 11 are asymptotic to a line of slope equal to 1, indicating that the shock is very nearly straight.

For positive angles of incidence, the shock wave must undergo a transition from the shape induced by the blunt leading edge to the shape determined by the shock generator. Here the shape induced by the shock generator is a straight line of angle determined using oblique shock wave theory for the appropriate flow turning angle. The trend exhibited by the shock shape curves is that, as angle of incidence increases, the shock becomes less curved at the same X/D.

The shock waves resulting from the sharp, .635 cm (.250 in) and 1.27 cm (.500 in) diameter leading edges at incidences of 0° and 10° are shown in Figures 16, 17 and 18, respectively. The shock waves for the sharp leading edge are at angles evaluated using oblique shock wave theory with the zero incidence case being a Mach Wave at the appropriate angle.

4.3 Surface Pressure Distributions

In presenting and analyzing such data, several possible coordinate systems and/or scaling parameters are available. Similar to the analysis of two-dimensional interactions, the incoming boundary layer thickness has in the past been used to non-dimensionalize the streamwise distance coordinate (i.e. X_s/δ). If δ is assumed to be a scaling parameter, then strictly speaking, both the X and Y directions should be presented in non-dimensional form. In this study, the only comparison of pressure distributions which can be made for a fixed Y/δ is between the most inboard tap row of the Model 2 configuration and the furthest outboard of Model 1. Plots made of pressure distributions in terms of X_s/δ for a fixed Y/δ from both the sharp and blunted leading edge studies show that the data do not collapse in this coordinate system. This is clearly illustrated by the two pressure distributions shown in Figure 19. This figure shows data at an approximate Y/δ of 8 for leading edge bluntnesses of .305 cm (.120") and .318 cm (.125") from the thin and thick boundary layer studies respectively. Figure 20, which shows the same two plots in terms of absolute distance X_s, indicates that scaling X_s by δ results in no semblance of collapse.

A second possibility was suggested by the behavior of the shock shapes as a function of fin leading edge bluntness and incidence. For a given Mach number the shock shape and its location

depend only on the fin bluntness D and the incidence α_G. If inviscid effects predominated, it might be anticipated that the pressure distributions would scale using a coordinate system nondimensionalized by the fin leading edge bluntness, D.

Figures 21, 22, and 23 each show five pressure distributions plotted as a function of X_s, X_s/δ and X_s/D, respectively. These distributions correspond to a mean (Y/D) of 8.7 and were obtained for a fin incidence of 10°. Four of these distributions are from the Model 1 study (thick boundary layer) with the other from the Model 2 study (thin boundary layer). Each distribution was measured along a different pressure tapping row with a different fin leading edge bluntness. The only common factor, a purely geometric one, is that the mean value of (Y/D) is about 8.7.

From the three figures it can be seen that the obviously separate distributions obtained when plotted in terms of X_s, or X_s/δ, can be collapsed when presented in terms of X_s/D. The predominantly inviscid characteristic of the interaction in this region is forcefully illustrated by this collapse. In this purely geometric coordinate system, the pressure distribution is clearly independent of the incoming boundary layer thickness. As seen above, the figure encompasses both Model 1 and 2 studies involving incoming boundary layers with thicknesses in the ratio of about 4:1. The same series of plots as illustrated by Figures 21, 22 and 23, was constructed over the entire incidence range for this same Y/D of about 8 . In all cases, a good collapse of the data was obtained when scaled by D. Similarly, checks were made at incidences of 4° and 10° for the two sets of data in the Model 1 study having a mean (Y/D) of about 4. Again, an excellent collapse was obtained for data plotted in terms of X_s/D.

All of the data referred to above fell in a region of the interaction where the shock wave shape is dominated by the generator nose. This region, extending about 10D downstream of the nose and about 10D outboard of it, is clearly shown in the shock shape plot of Figure 11. Further downstream of and outboard of this region the generator incidence starts to play a role in determining the shock shape. Evidently, even further downstream and outboard of this transition area, the shock wave will become the oblique shock wave corresponding to the flow turning angle dictated by the main body of the fin.

A second series of pressure distributions, plotted as functions of X_s, X_s/δ and X_s/D has been made for a mean Y/D of 31 for a shock generator incidence of 10°. These are shown in Figures 24, 25, and 26, respectively. From the above discussion, it can be seen that a Y/D of 31 falls in what has been referred to as the transition region of the interaction.

In these three figures, four of the pressure distributions are from the thin boundary layer study (Model 2) and one is from the thick boundary layer study (Model 1). The collapse of these data is poor compared to the collapse for a Y/D of 8.7. It would seem that with increasing distance along the shock wave (in terms of D) the strongly inviscid character of the interaction starts to change. This transition region, obviously occurring in the range Y/D between 8 and 31, will be closely examined in the full analysis of the data, planned as the next phase of this study. In conjunction with the 'sharp' study and any necessary supporting measurements, the different regions of the interaction, their character, and their controlling parameters should be identifiable.

A closer examination of the data shown in Figures 21 to 26 provides further support for the concept of the interaction being primarily inviscid. For the five pressure distributions presented on any one of these plots, data are shown for Model 1 and 2 configurations which not only have the same Y/D but have almost the same components Y and D, i.e. for Y/D = 8.7.

Model 1: Y = 2.66 cm (1.05"), D = .318 cm (.125")
Model 2: Y = 3.29 cm (1.29"), D = .406 cm (.160")

Since these data collapse in terms of X_s/D (figure 23), and they have almost the same value of D, then they must also collapse in terms of X_s alone. This collapse, which is particularly good, can be seen by referring back to Figure 21. For these two interactions the incoming boundary layers have thicknesses in the ratio of almost 5:1, yet the pressure distributions as a function of absolute distance are almost identical. In terms of δ, the incoming boundary layer thickness, the streamwise extent of the interaction is about 10δ in the Model 1 case and about 50δ in the Model 2 case. In absolute terms, the streamwise extent for both is approximately 12.5 cm (5"). Scaling X_s by δ, as shown in Figure 22, only distorts and separates these distributions as is readily obvious from the above remarks on the interaction length. This independence of incoming boundary layer thickness (or local Reynolds number), strongly suggests an inviscid governing mechanism, rather than one resulting from the mutual interaction between the external inviscid flow and the boundary layer itself.

4.4 Oil Flow Patterns

The test matrix for surface oil flow data was identical to that for surface pressure distributions (figure 1). This included the sharp leading edge configuration. The oil flow photographs were taken with the pressure plates as the test surface. Pressure tappings served as points of reference for determination of the surface oil flow angle and measurements were taken along

these rows. This provided consistency as well as ease in data analysis, since the location of each pressure tapping was known in the X_s, X_s/δ and X_s/D coordinate systems. The technique provided a picture of the entire surface flow region visible through the optical window.

Surface flow angles have been examined for values of Y/D of approximately 8.7 and 31. These were selected to check whether the surface oil flow angles would scale in a manner similar to the surface pressures. Data at these Y/D values were examined in both the X_s/δ and X_s/D coordinate systems to offer a more complete comparison with results obtained in the surface pressure distribution part of the investigation. Surface oil flow angles at $Y/D \simeq 8.7$ for a shock generator incidence of 10° are shown in Figures 27 and 28 in X_s/δ and X_s/D coordinates, respectively. The scaling of the interactions by δ, as in Figure 27, does not result in a collapse of the curves. The Model 2 (thin boundary layer) curve for $Y/D \simeq 8.7$ (the solid line of Figure 27) was shifted well away from those of the Model 1 (thick boundary layer) case at $Y/D \simeq 8.7$ because of scaling by the smaller δ. In this figure, the region for data acquisition allowed by the optical window for each leading edge diameter can be easily seen. When moving from the shock generator outwards (increasing Y direction), the length of the interaction region visible through the optical window along the X_s axis progressively increased.

The same data of Figure 27 scaled by the leading edge diameter, D, is shown in Figure 28. The collapse of the data in this form is excellent and is consistent with the surface pressure data from the identical locations (shown previously in Figure 23). This supports the validity of the leading edge diameter as a scaling parameter in this region and further demonstrates the inviscid character of this type of three-dimensional interaction.

Figures 29 and 30 present surface oil flow data for the five leading edge diameters having values of Y/D near 31. When scaled by δ (figure 29) similar trends are seen to exist, but a collapse of the data does not result. The solid line representing the surface oil flow angles of the Model 1 interaction, D = .318 cm (.125 in) at $Y/D \simeq 31$ lies well inside of the others, all of which are from the Model 2 (thin boundary layer) configuration. This results from nondimensionalization of X_s by the larger value of δ. When these interactions are scaled by the leading edge diameter, the scaling is superior to that offered by δ, but is poorer than that at $Y/D \simeq 8.7$. As is the case at $Y/D \simeq 8.7$, the surface oil flow angles at $Y/D \simeq 31$ are consistent with the surface pressure measurements.

4.5 Heat Transfer Rate Measurements

No analysis has been made so far on the heat transfer rate measurements. This will be carried out in the full analysis planned as the next phase of this program. All of the measurements have been made and the raw data assembled in the data bank. The locations of the shock based origins $X_s = 0$ have been obtained and the slug coordinates in the X_s, X_s/δ and X_s/D systems are currently being evaluated. Heat transfer data are being stored in the form of the ratio of the local heat transfer rate coefficient to the undisturbed value ahead of the interaction. The latter has been estimated from the van Driest II skin friction correlation using a Reynolds analogy factor of 1.2.

The slug calorimeter method used here is very similar to the better known "thin skin" technique, but unlike the latter which is generally used in short duration fast start facilities, the slug calorimeter is suitable for use under continuous flow conditions. Each slug is fitted with an external intermittent heating source which is used to raise its temperature above the wall temperature during tunnel operation. On cutting off the heat input to the slug its temperature time history was recorded from which the heat transfer rate $\dot{q}_w$ could be calculated

$$q_w = \frac{m_s C_s}{A_s} \left[\frac{dT_s}{dt}\right]_{t=t_o}$$

with $(dT_s/dt)_{t=t_o}$ being evaluated when the slug temperature was equal to the wall temperature.

All measurements were made with the wall at a uniform temperature. This is ensured by the tunnel construction which uses 6.35 cm (2.5") thick aluminum walls. It is an inherent operating characteristic of the tunnel that the stagnation temperature (and therefore the recovery and wall temperatures) decreases during a run. However, the decrease during the data taking part of a run (at maximum 5s) is small. To obtain the heat transfer coefficient from the absolute rate $\dot{q}_w$ the driving potential $(T_r - T_w)$ is used in the nondimensionalizing process.

$$\text{i.e.} \quad C_H \doteq \dot{q}_w / [\rho_\infty U_\infty C_p (T_r - T_w)]$$

Without recourse to either heated or cooled models the driving potential $(T_r - T_w)$ in the tunnel is typically 30°C to 40°C. This calls for accurate knowledge of the stagnation and wall temperatures since a 1°C overestimate in the former and 1°C underestimate in the latter will result in an error of about 7% in C_H. In all

cases the recovery temperature was calculated from the measured stagnation temperature using a recovery factor of .89.

A typical example of the heat transfer data as a function of X_s is plotted in Figure 31. These data are for a bluntness of .95 cm (.375") for incidences of 2°, 6°, 8° and 10°. It can be seen that the heat transfer rate stays at the undisturbed value right up until the shock wave location. In contrast, the pressure distribution for these conditions show the initial pressure rise to occur about 6.7 cm (2.6") ahead of the shock wave and in the 10° case rising to a pressure ratio of about 1.5 at the shock wave. This is quite different from the two-dimensional interaction where both pressure and heat transfer rate rise almost simultaneously some distance ahead of the shock wave location.

These aspects of the distributions, and in particular the use of different scaling parameters will be examined in detail in the next phase of the program.

4.6 Concluding Remarks on the Preliminary Data Analysis

From the preliminary analysis carried out so far, some very interesting and important results have emerged. These have provided considerable insight into the nature of different regions of this type of interaction.

The collapse of the data when scaled by D, even for cases with incoming boundary layers with thickness ratios of almost 5:1, shows conclusively the inviscid character of the interaction. Tentatively, it would appear that this type of scaling starts to break down with increasing distance (in terms of D) away from the shock generator. Since a range of Y/D from about 2 to 110 was covered in this study, it is hoped that, in the full analysis to be started shortly, the region in which this scaling is valid should be delineated. It would also seem that the use of the incoming boundary layer thickness as a scaling factor is inappropriate for any region of the interaction.

The three-dimensional interaction, long considered as the logical extension of the current computational thrust aimed at the two-dimensional case, may need a totally different and relatively simpler approach. If the two- and three-dimensional interactions are inherently different phenomena, it may be more logical to attempt prediction of the latter without waiting for successful prediction of the former.

REFERENCES

1. Winkelmann, A. E., "Flow Visualization Studies of a Fin Protuberance Partially Immersed in a Turbulent Boundary Layer at Mach 5", Naval Ordnance Laboratory Report NOLTR-70-93, May 1970.

2. Winkelmann, A. E., "Experimental Investigations of a Fin Protuberance Partially Immersed in a Turbulent Boundary Layer at Mach 5", Naval Ordnance Laboratory Report NOLTR-72-33, January 1972.

3. Sedney, R. & Kitchens, C. W., "The Structure of Three-Dimensional Separated Flows in Obstacle-Boundary Layer Interactions", USA Ballistic Research Laboratories Report BRL R 1791, June 1975.

4. Sedney, R. & Kitchens, Jr., C. W., "Measurement and Correlation of Separation Ahead of Protuberances in a Turbulent Boundary Layer", AIAA Paper 76-163, AIAA 14th Aerospace Sciences Meeting, Jan. 26-28, 1976.

5. Korkegi, R. H., "Investigation of Small Surface Protuberances Upstream of Turbulent Boundary Layer Separation Produced by a Skewed Shock Wave at Mach 3", Air Force Aero Propulsion Laboratory AFAPL-TR-76-16, May 1976.

6. Sedney, R. and Kitchens, Jr., C. W., "Separation Ahead of Protuberances in Supersonic Turbulent Boundary Layers", BRL R 1958, February 1977.

7. Price, A. E. & Stallings, R. L., "Investigation of Turbulent Separated Flows in the Vicinity of Fin Type Protuberances at Supersonic Mach Numbers", NASA TN D-3804, February 1967.

8. Gillerlain, J. D., "Experimental Investigation of a Fin Cone Interference Flow Field at Mach 5", Naval Surface Weapons Center Report NSWC/NOL/TR 75-63.

9. Gillerlain, J. D., "Use of Phase Change Paints to Study Fin Body Interference Heating", Naval Surface Weapons Center Technical Report NSWC/WOL/TR 75-62, April 1976.

10. Kaufmann, II, L. G., Korkegi, R. H. & Morton, L. C., "Shock Impingement Caused by Boundary Layer Separation Ahead of Blunt Fins", ARL 72-0118, August 1972.

11. McCabe, A., "A Study of Three-Dimensional Interactions Between Shock Waves and Turbulent Boundary Layers", Ph.D. Thesis, University of Manchester, 1963.

12. Lowrie, B. W., "Cross Flows Produced by the Interaction of a Swept Shock Wave with a Turbulent Boundary Layer", Ph.D. Thesis, University of Cambridge, 1965.

13. Token, K. H., "Heat Transfer Due to Shock Wave Turbulent Boundary Layer Interactions on High Speed Weapons Systems" AFFDL-TR-74-77, 1974.

14. Peake, D. J., "The Three-Dimensional Interaction of a Swept Shock Wave with a Turbulent Boundary Layer and the Effects of Air Injection on Separation", Ph.D. Thesis, Carleton University, Ottawa, 1975.

15. Oskam, B., Bogdonoff, S. M., & Vas, I. E., "Study of Three-Dimensional Flow Fields Generated by the Interaction of a Skewed Shock Wave with a Turbulent Boundary Layer", AFFDL-TR-75-21, February 1975.

16. Oskam, B., "Three-Dimensional Flow Fields Generated by the Interaction of a Swept Shock Wave with a Turbulent Boundary Layer", Princeton University Gas Dynamics Laboratory Report 1313, December 1976.

17. Oskam, B., "Three-Dimensional Flow Fields Generated by the Interaction of a Swept Shock Wave with a Turbulent Boundary Layer", Ph.D. Thesis, Dept. of Aerospace & Mechanical Sciences, Princeton University, 1976.

18. Hayes, J. R., "Prediction Techniques for the Characteristics of Fin Generated Three-Dimensional Shock Wave Turbulent Boundary Layers", AFFDL-TR-77-10, May 1977.

19. Liepman, H. W. & Roshko, A., Elements of Gas Dynamics, Wiley and Sons, New York, 1957.

20. Vas, I. E. & Oskam, B., "Heat Transfer Measurements Using the Quasi-Transient Technique", Presented at the 45th Semi-Annual Meeting of the Supersonic Tunnel Association, Albuquerque, New Mexico, April 13-14, 1976.

21. Baradell, D. L. & Bertram, M. H., "The Blunt Plate in Hypersonic Flow", NASA TN D-408, 1960.

BLUNTED STUDY TEST MATRIX

THICK BOUNDARY LAYER: $\delta = .50''$

BLUNTNESS D	Y/D AT PRESSURE TAPPING ROW			
	Y=0.9"	Y=1.9"	Y=2.9"	Y=3.9"
.125"	7.7	15.7	23.7	31.7
.250"	4.1	8.1	12.1	16.1
.375"	2.9	5.6	8.2	10.9
.500"	2.3	4.3	6.3	8.3

THIN BOUNDARY LAYER: $\delta = .15''$

BLUNTNESS D	Y/D AT PRESSURE TAPPING ROW			
	Y=1.15"	Y=2.15"	Y=3.4"	Y=4.4"
.040"	29.3	54.3	85.5	110.
.080"	14.9	27.4	43.0	55.5
.120"	10.1	18.4	28.8	37.2
.160"	7.7	13.9	21.8	28.0

FIGURE 1 BLUNTED STUDY TEST MATRIX

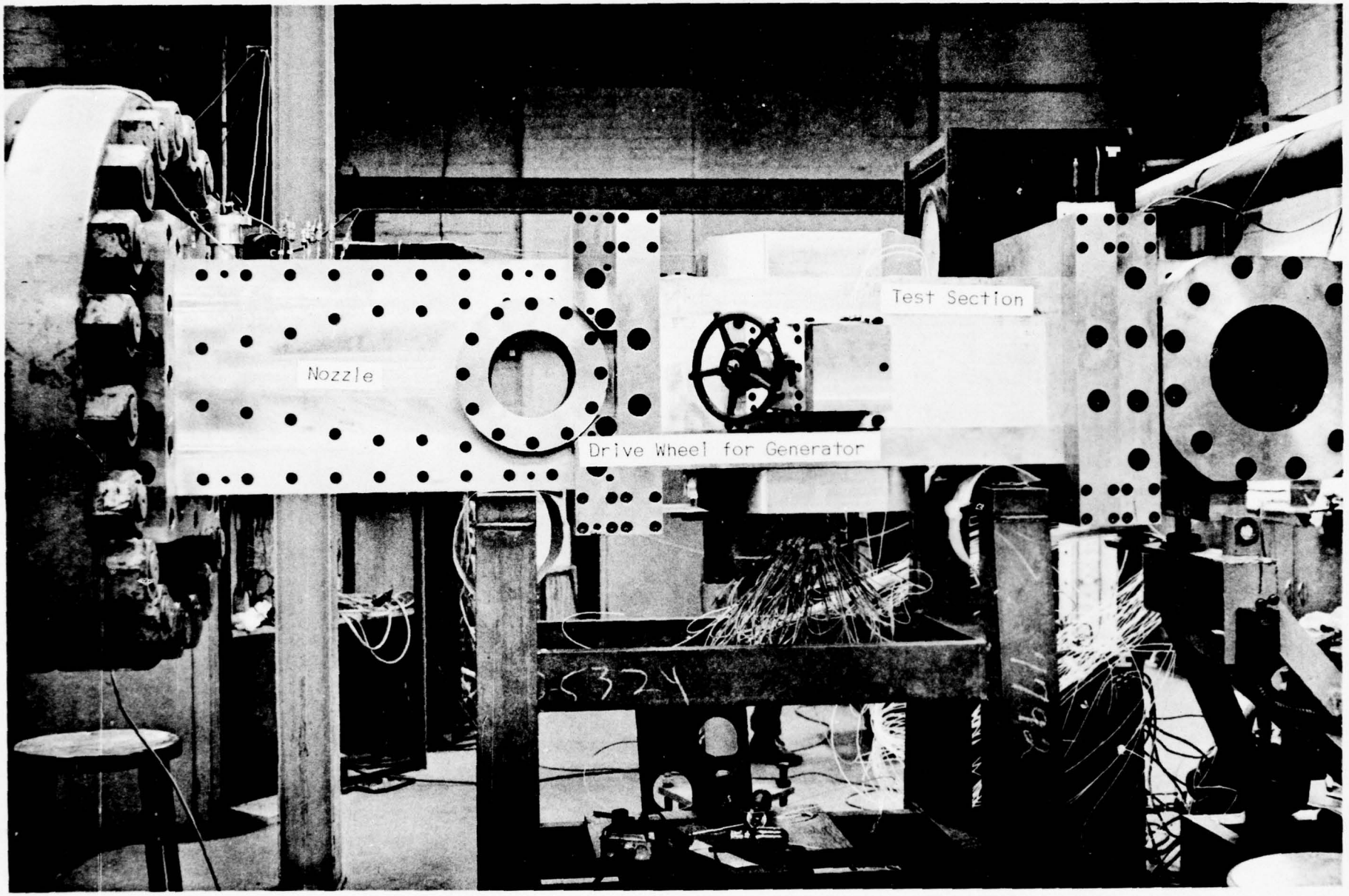

Figure 2. Photograph of Tunnel with Section for Three-Dimensional Shock Boundary Layer Interaction

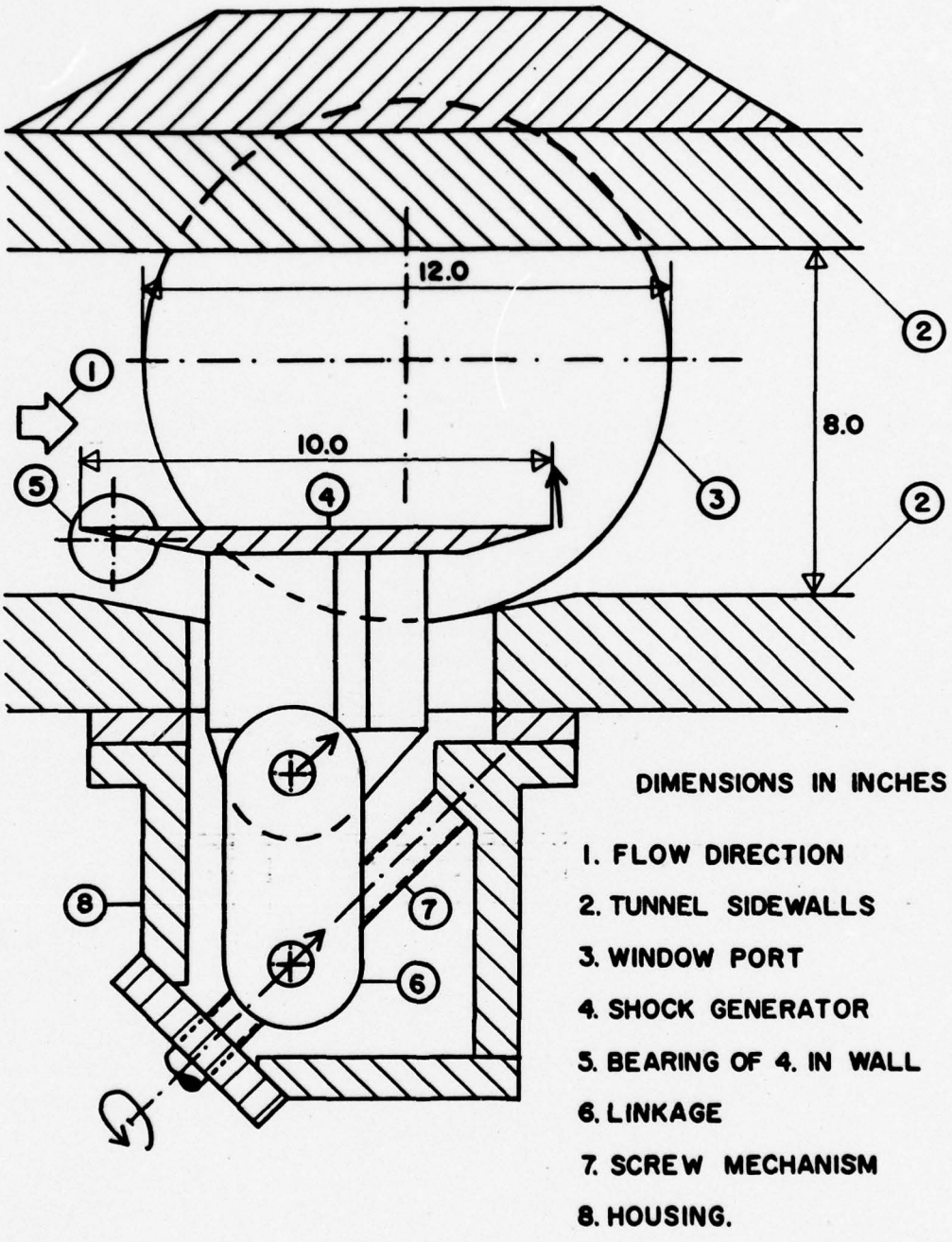

Figure 3. Line Drawing of Shock Generator Actuating Mechanism.

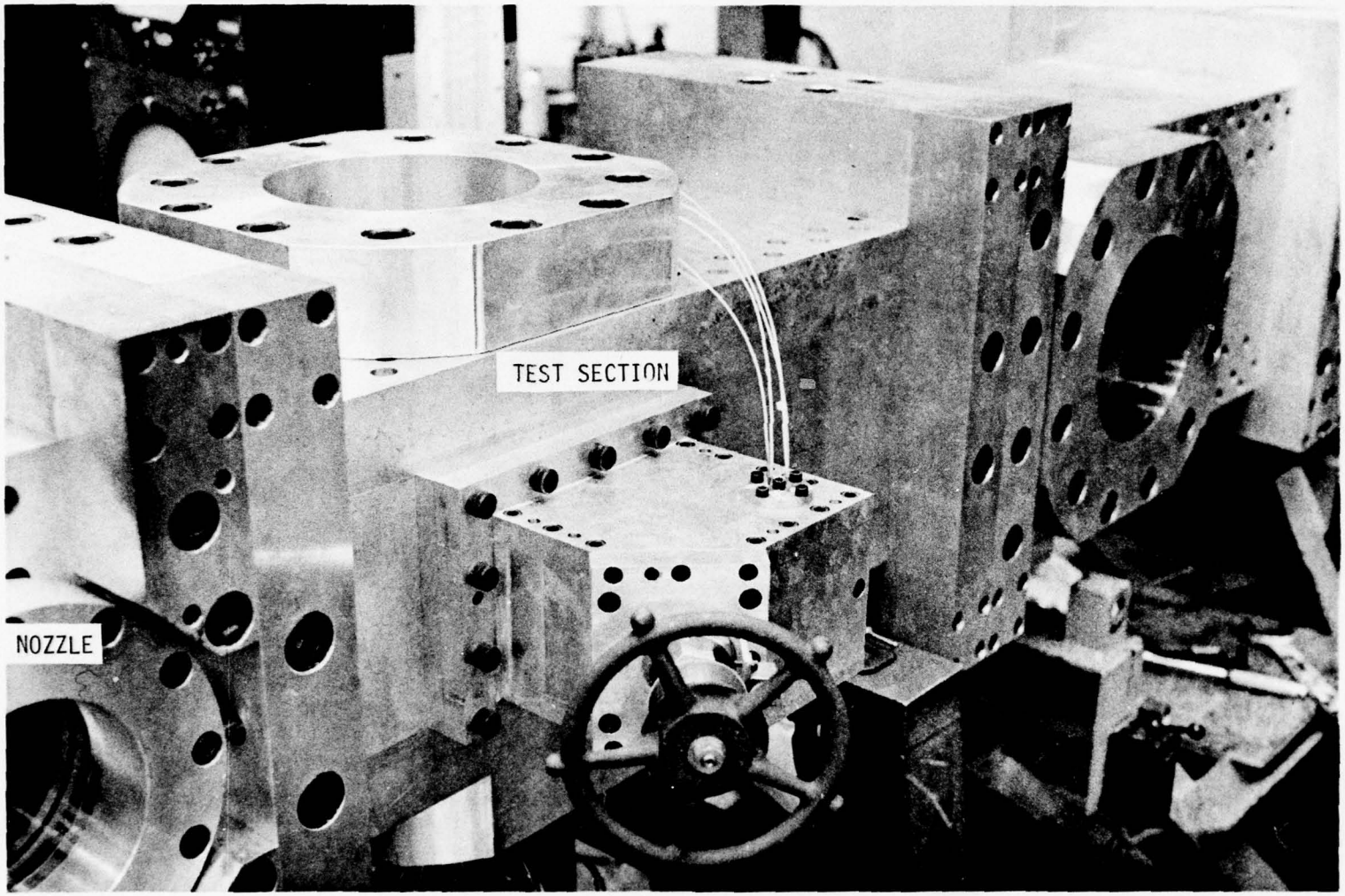

Figure 4. **Photograph of Wind Tunnel Test Section Installed Behind Nozzle Section.**

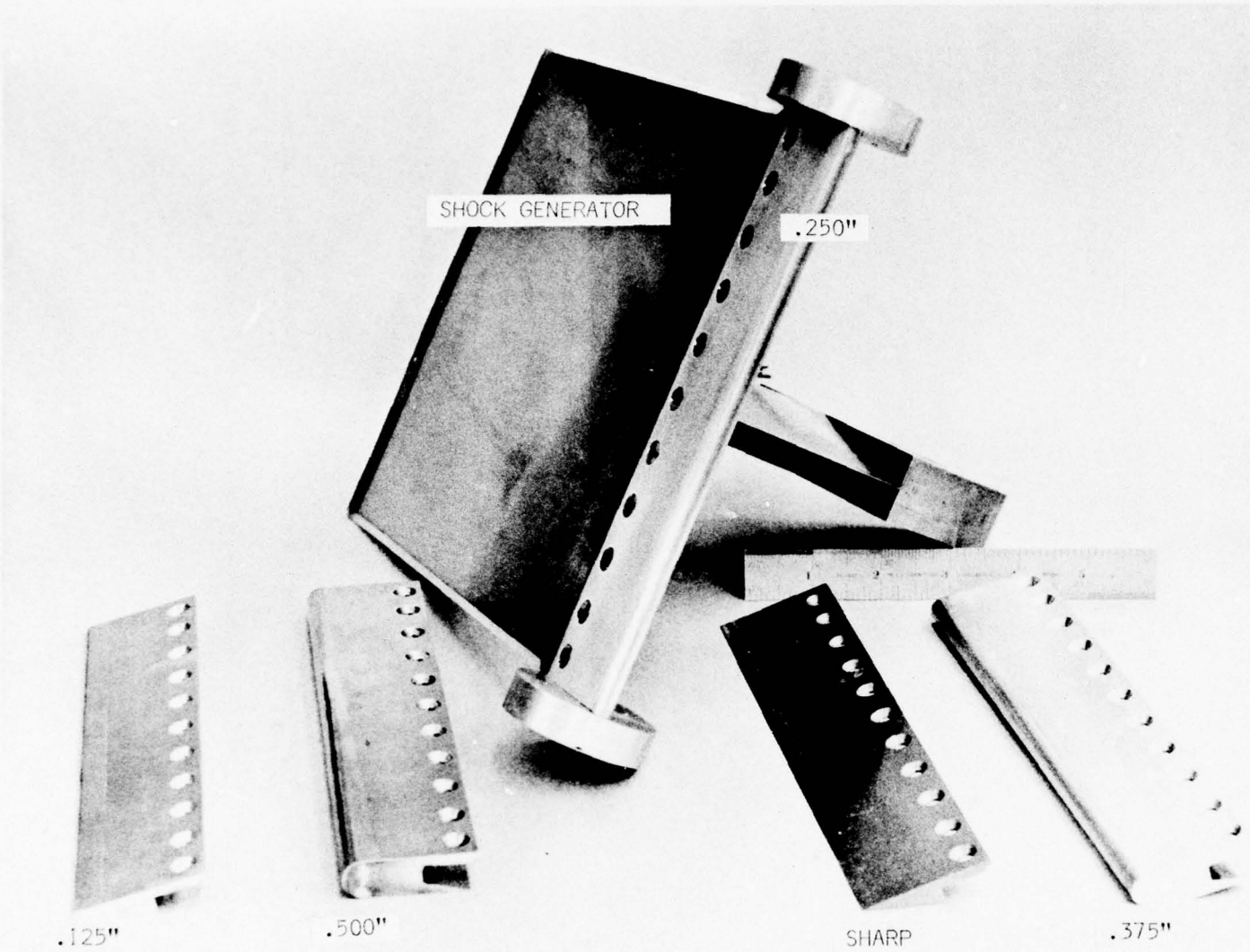

Figure 5. 8" Shock Generator with Various Leading Edge Bluntnesses.

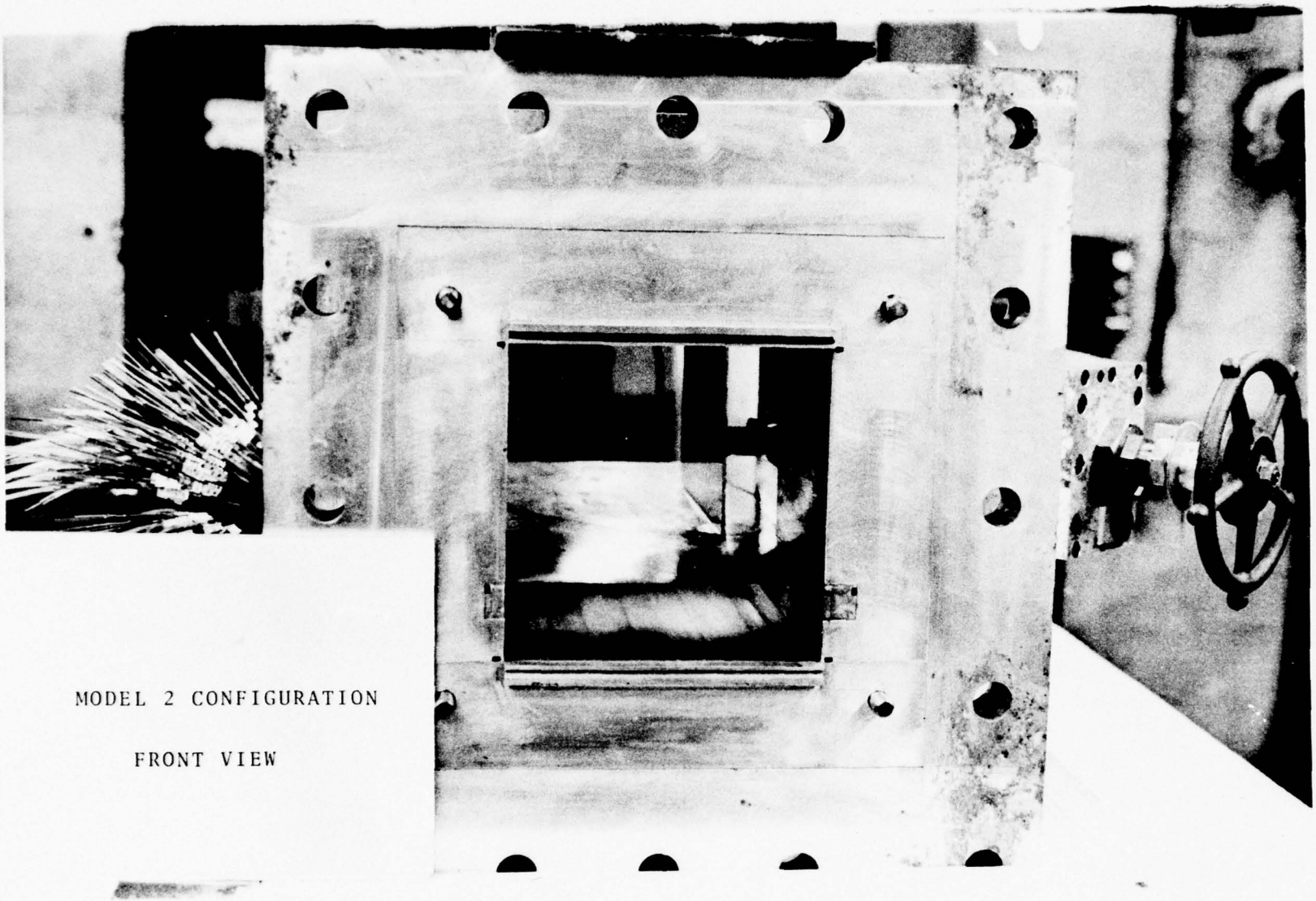

Figure 6. Model 2 Configuration Installed in the Test Section.

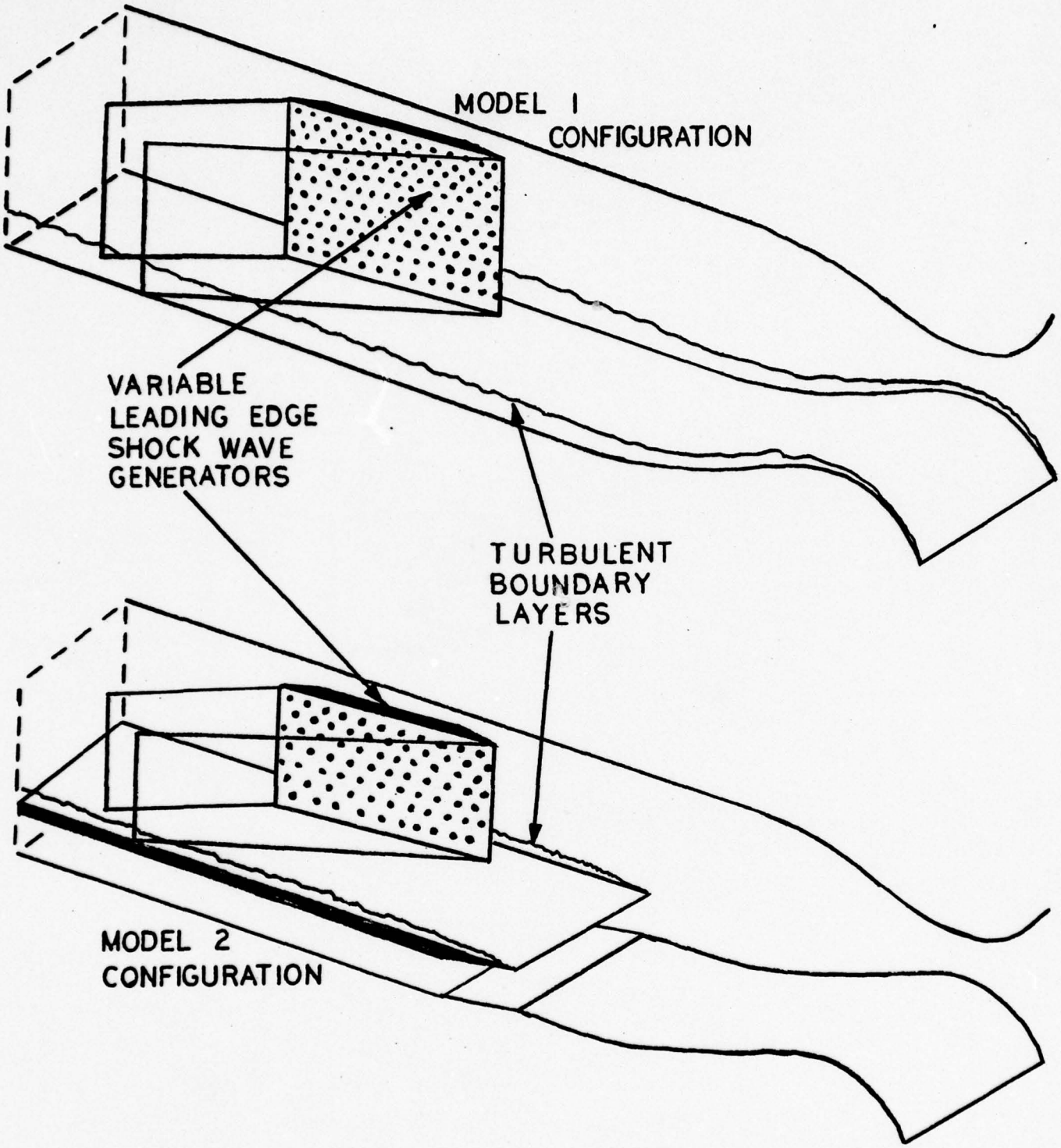

FIGURE 7 MODEL CONFIGURATIONS

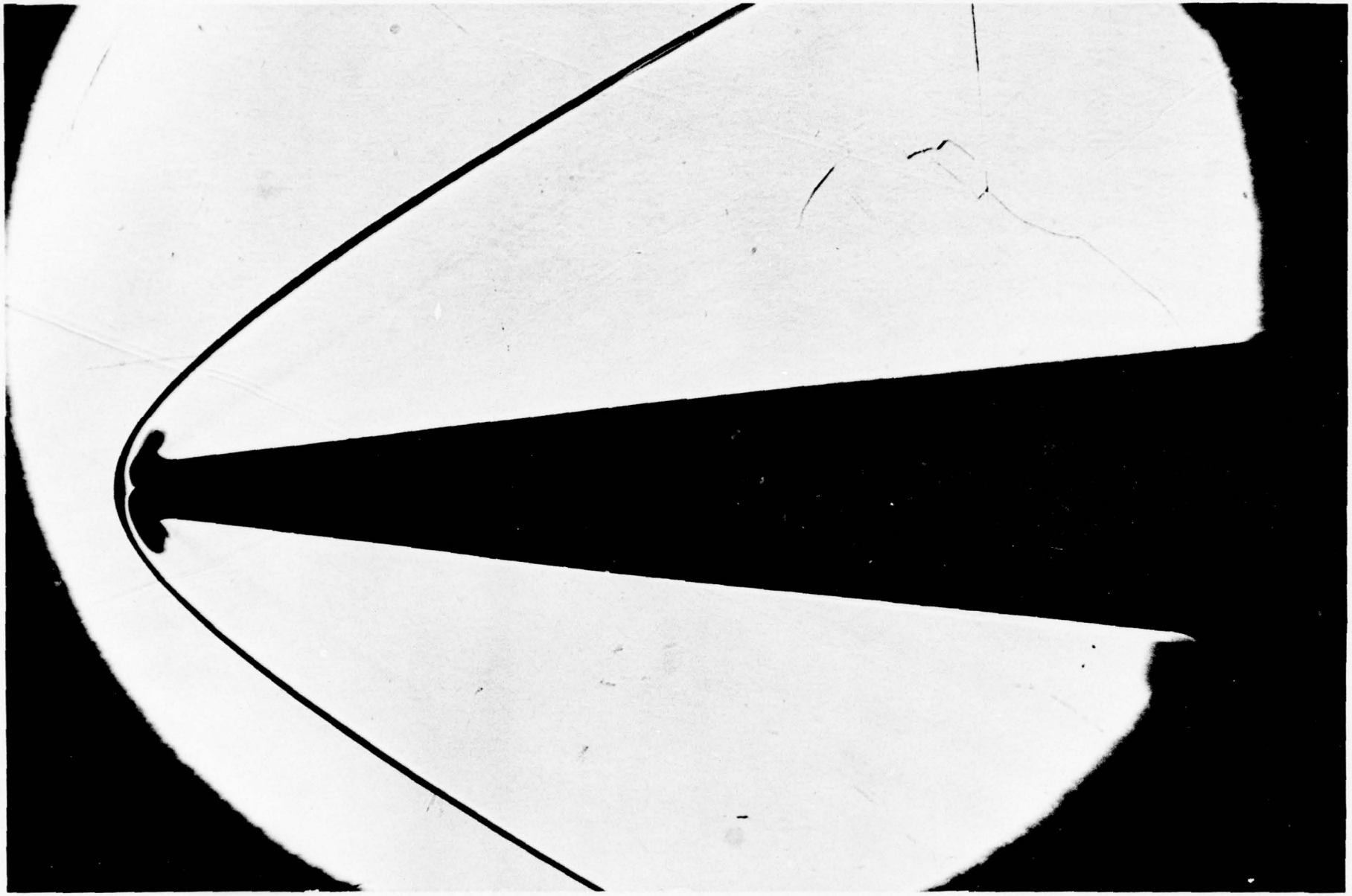

Figure 8. Shadow Photograph of Shock Shape for D = .635cm (.250"), $\alpha_G = 6°$.

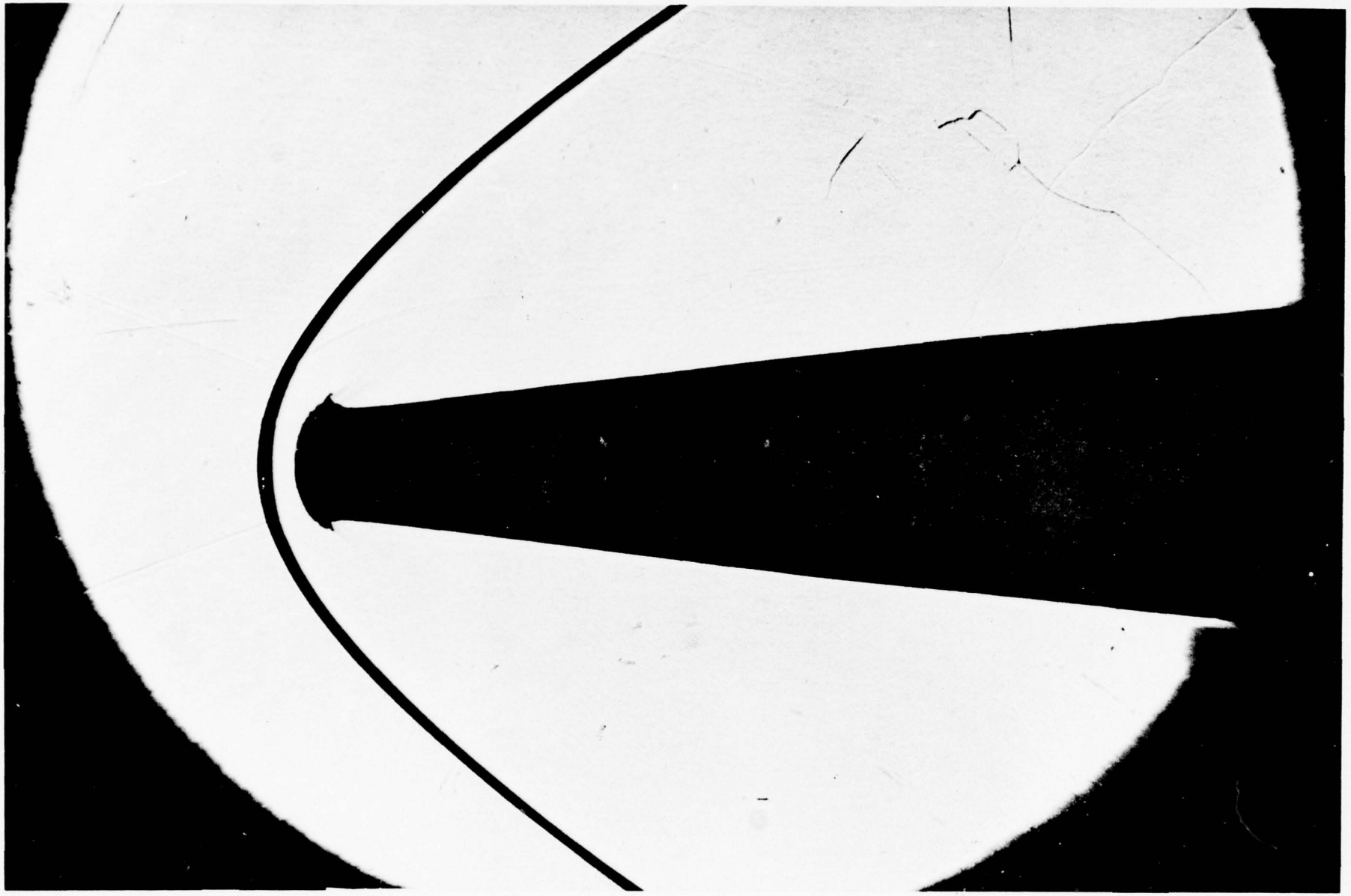

Figure 9. Shadow Photograph of Shock Shape for D = 1.27cm (.500"), α_G = 6°.

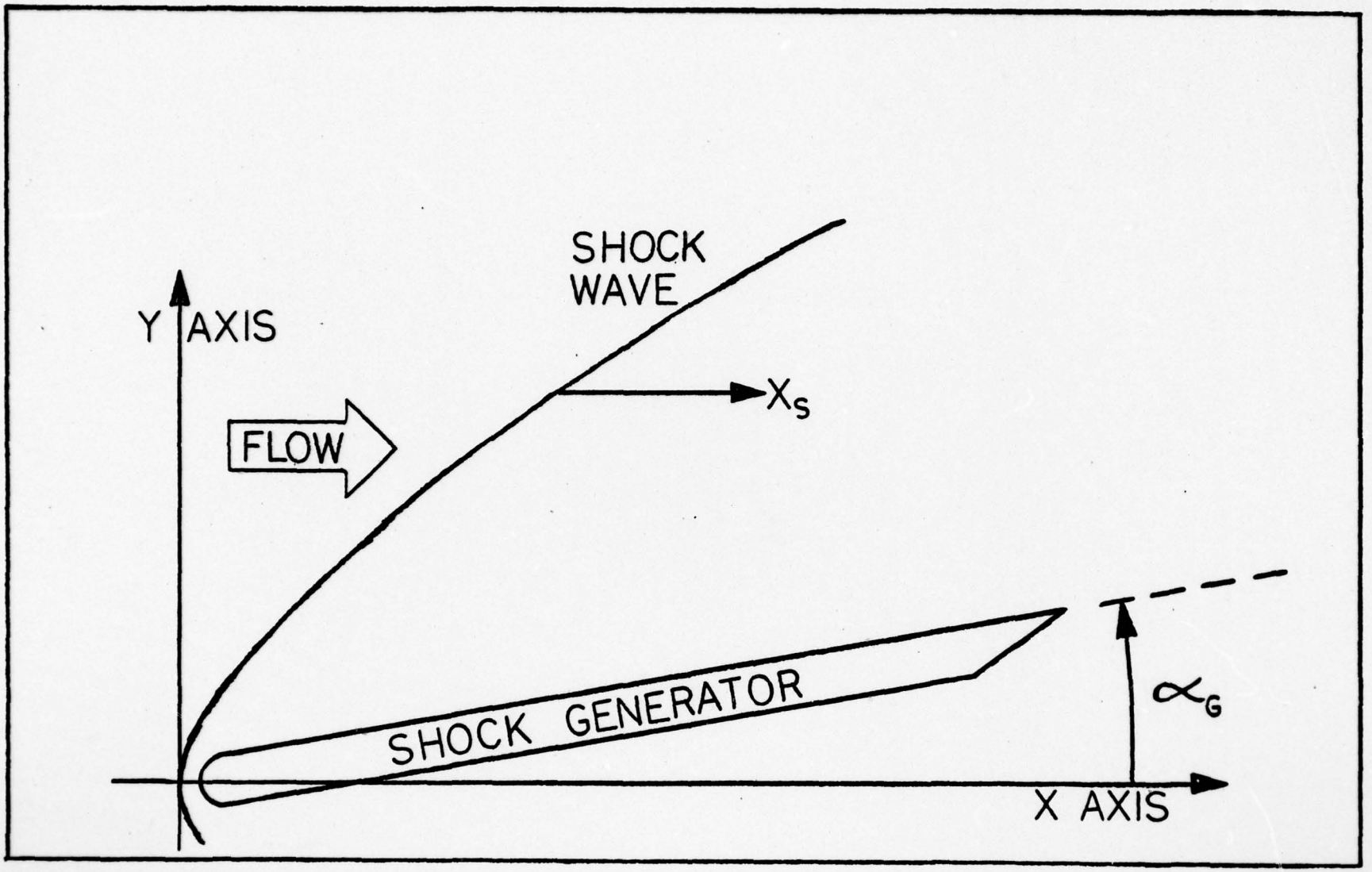

FIGURE 10 COORDINATE SYSTEMS

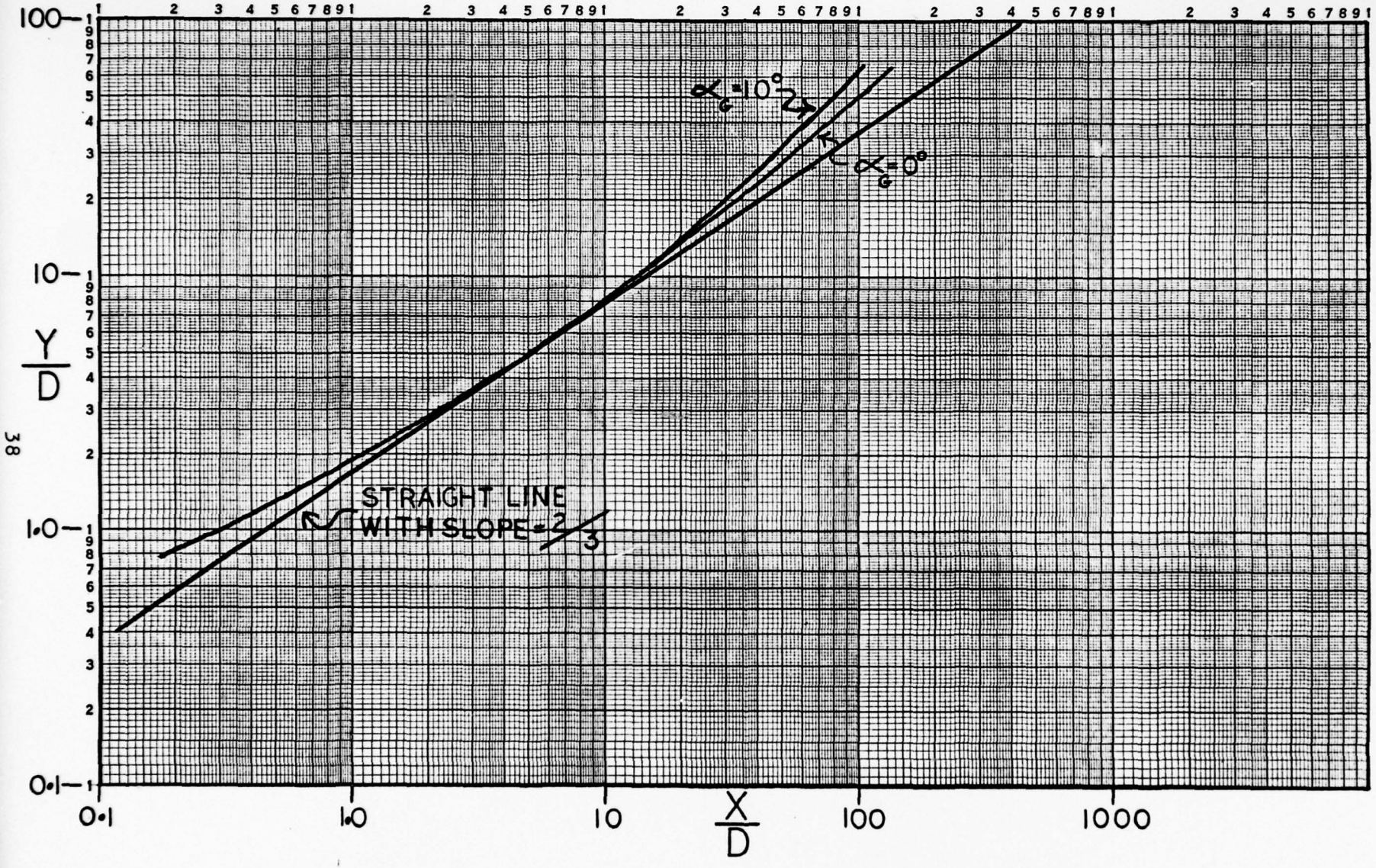

Figure 11. Shock Shapes in the Form Y/D vs. X/D for α_G = 0° and 10°.

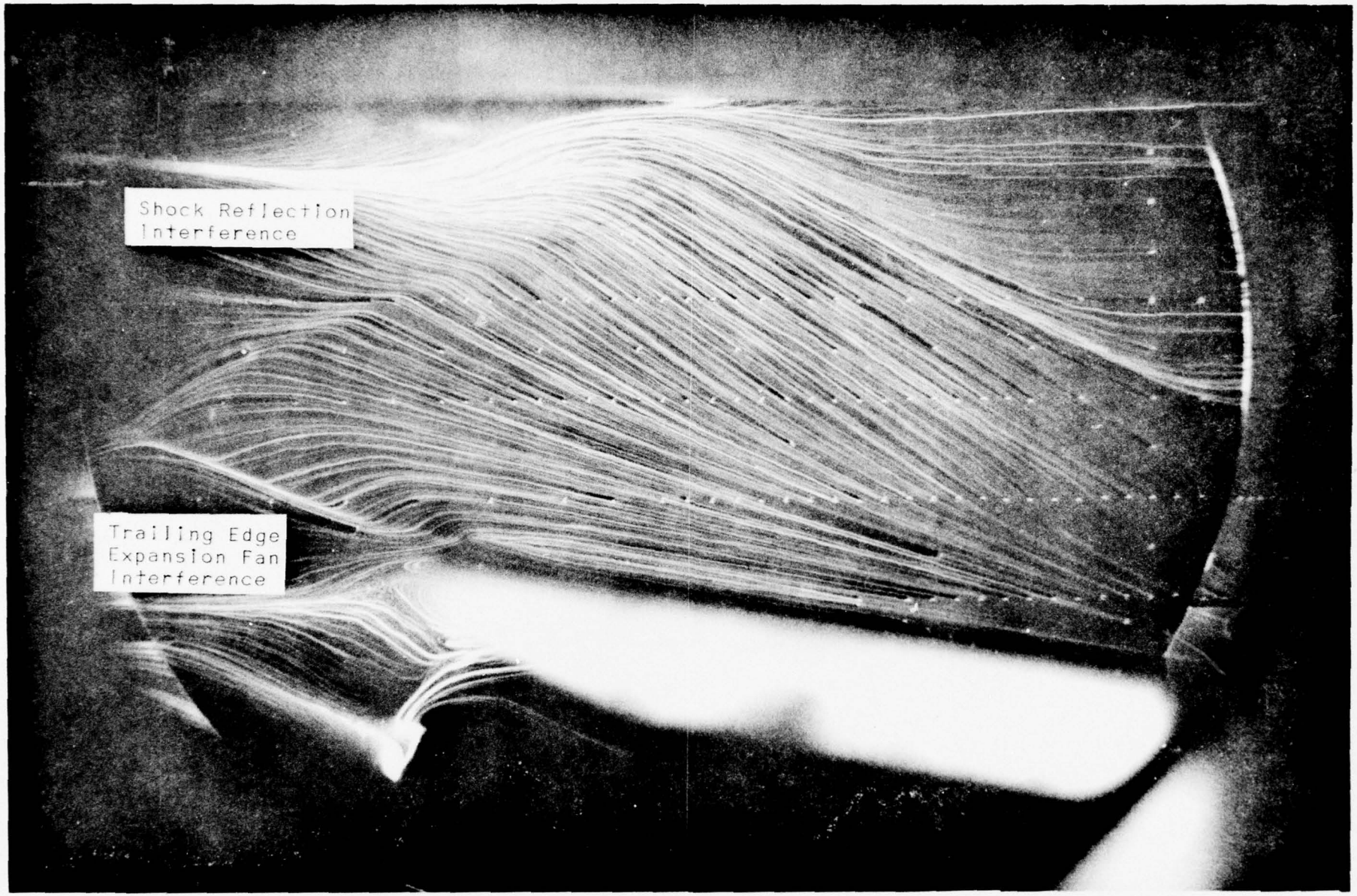

Figure 12. Oil Streak Pattern Illustrating Interference Effects.

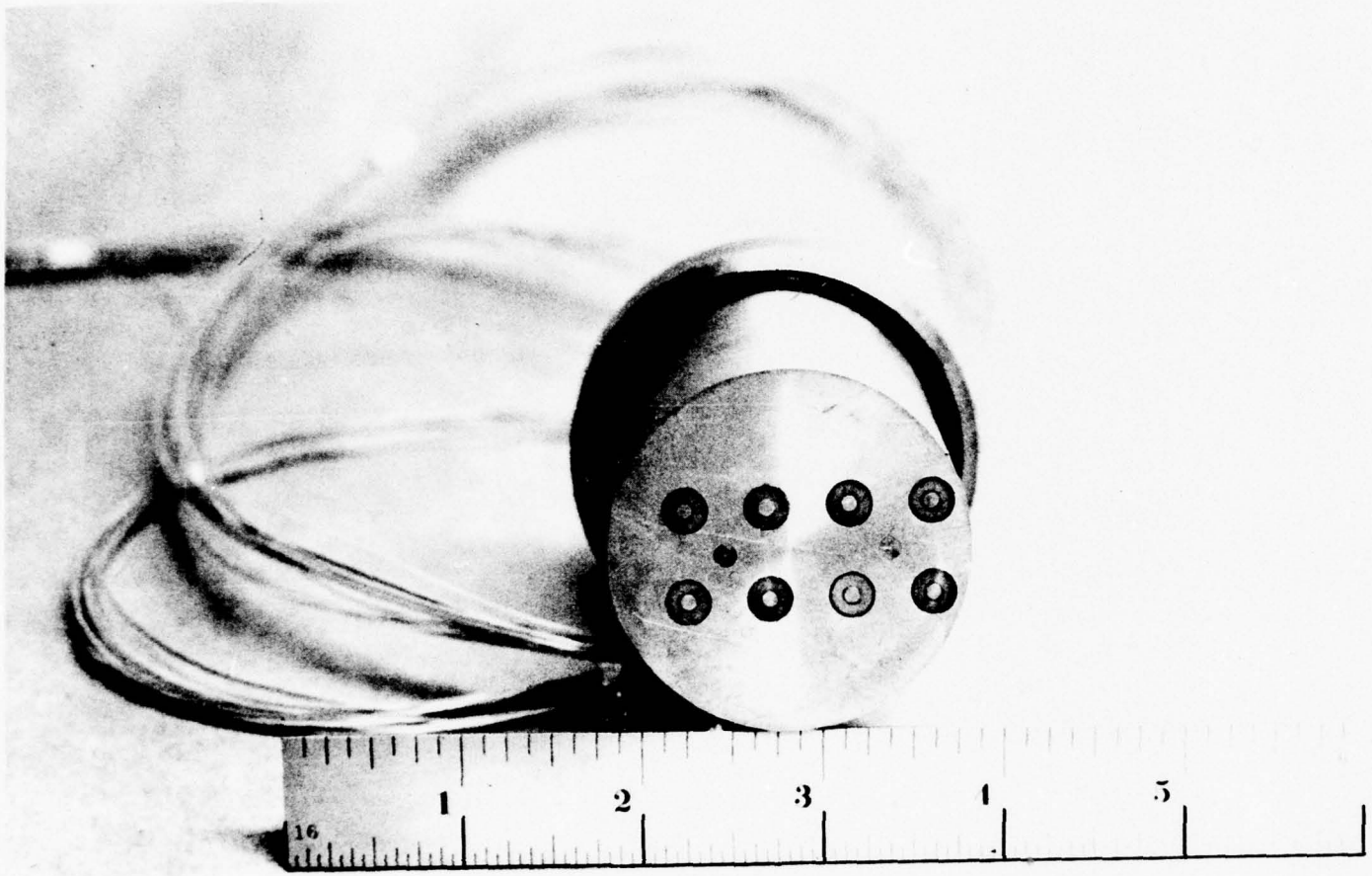

Figure 13. Photograph of Heat Transfer Plug No. III, Scale in Inches.

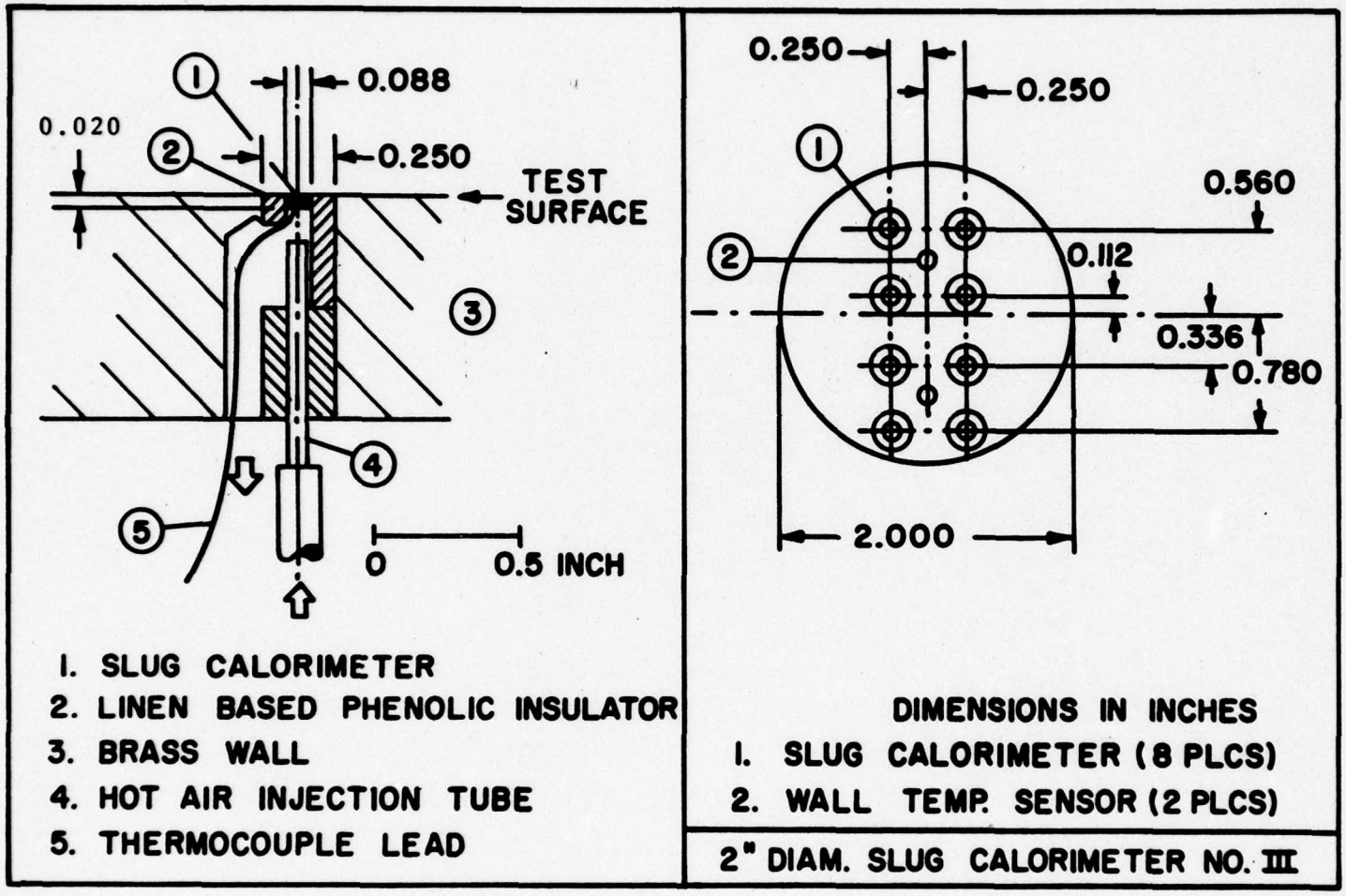

Figure 14. Drawing of Heat Transfer Instrumentation and Slug Calorimeter Detail.

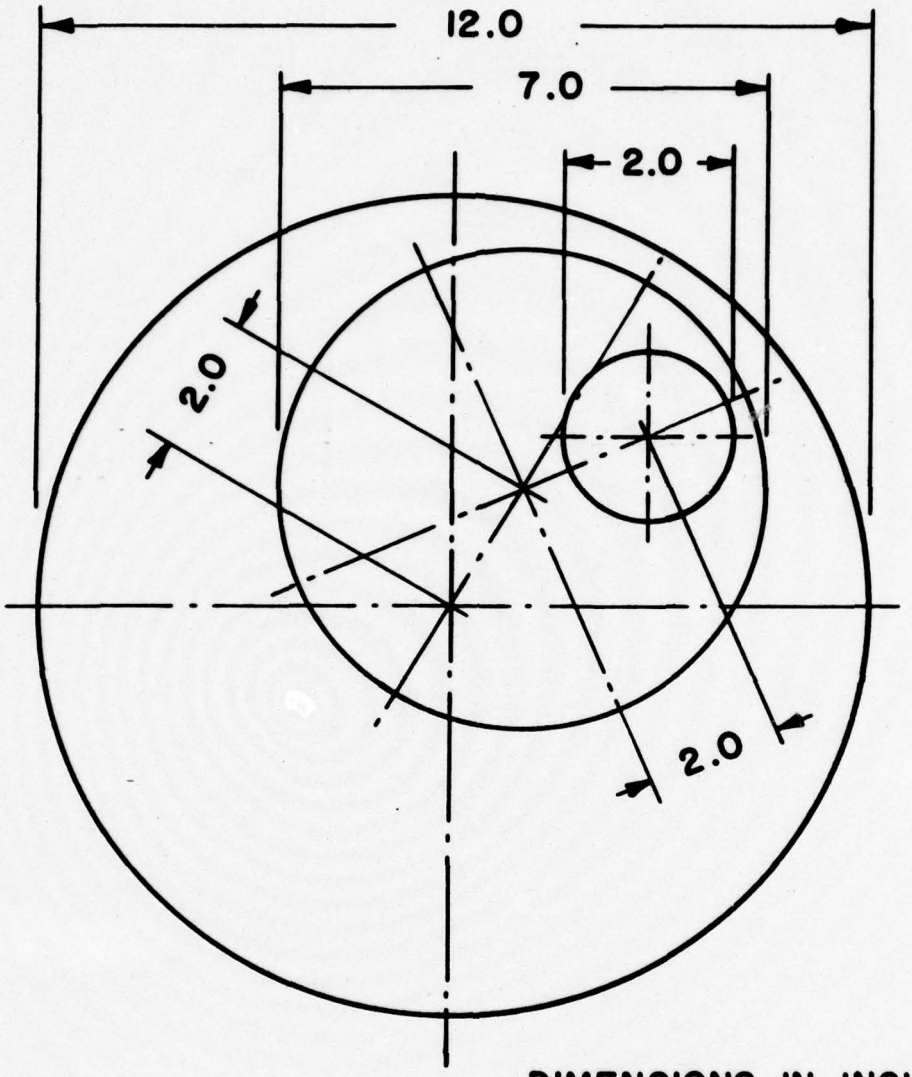

Figure 15. Line Drawing of Eccentric Rotatable System.

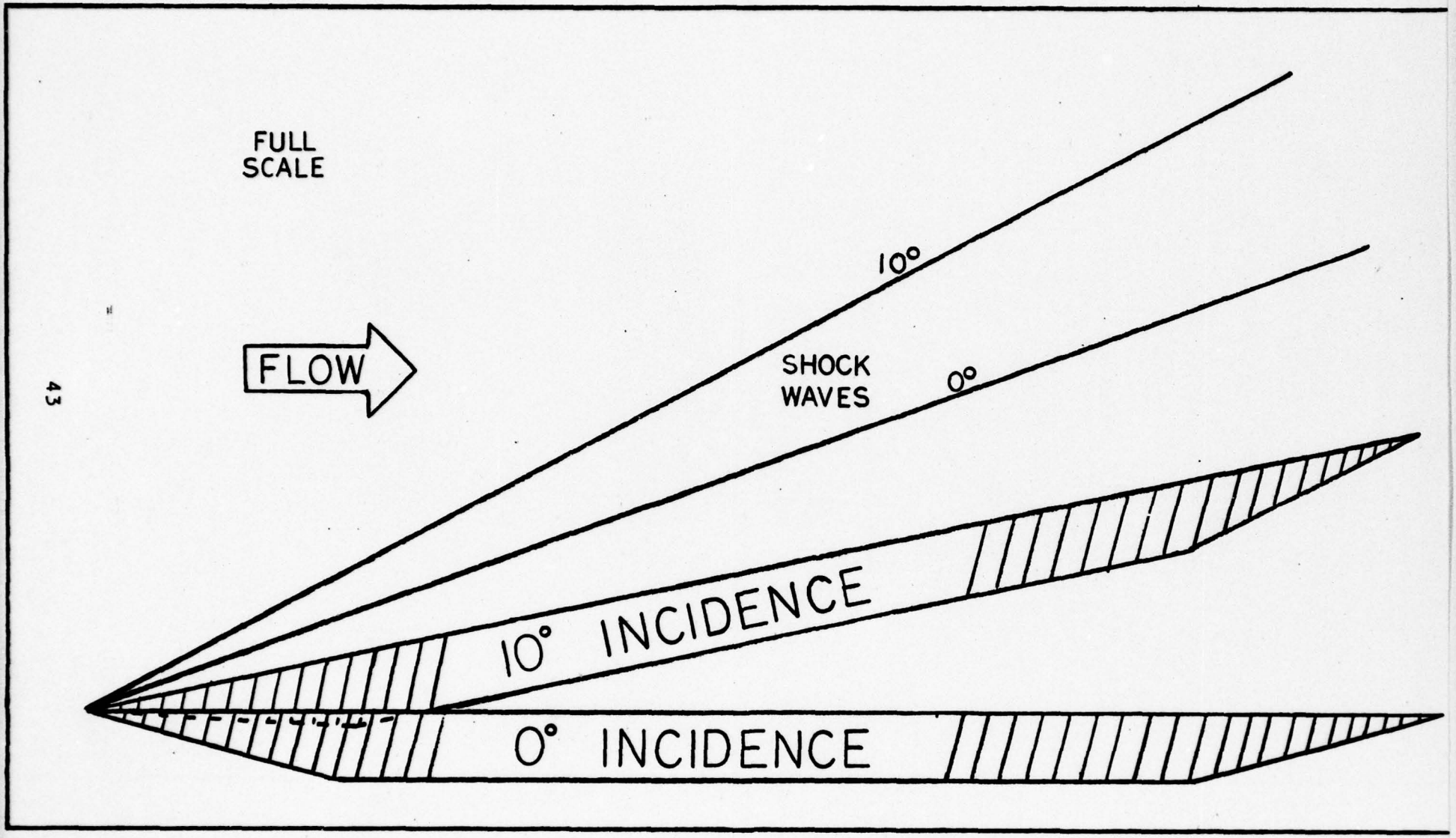

Figure 16. Effect of Incidence on the Theoretical Shock Wave Shape for the Sharp Leading Edged Generator.

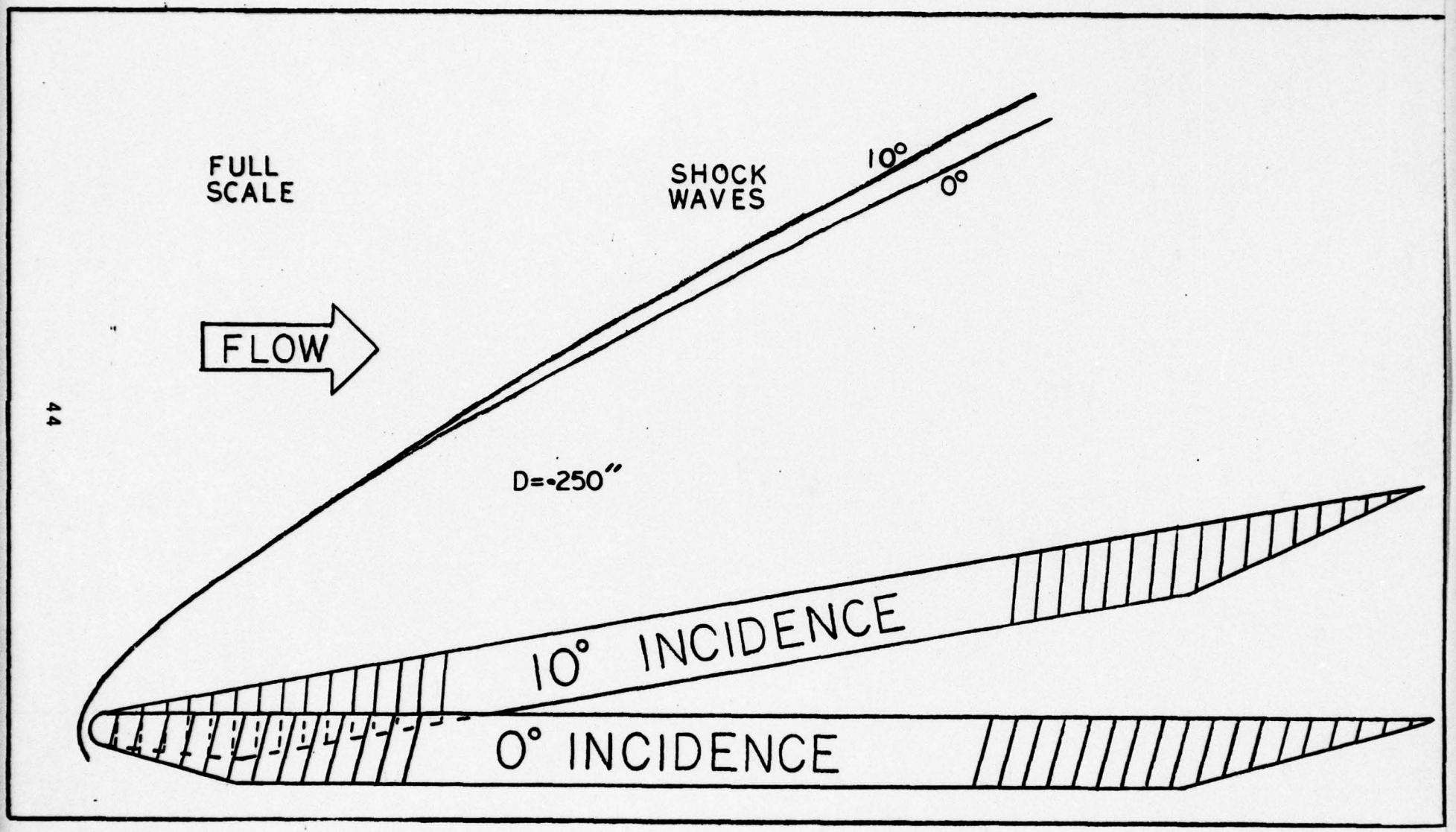

Figure 17. Effect of Incidence on the Observed Shock Wave Shape for D = .635cm (.250").

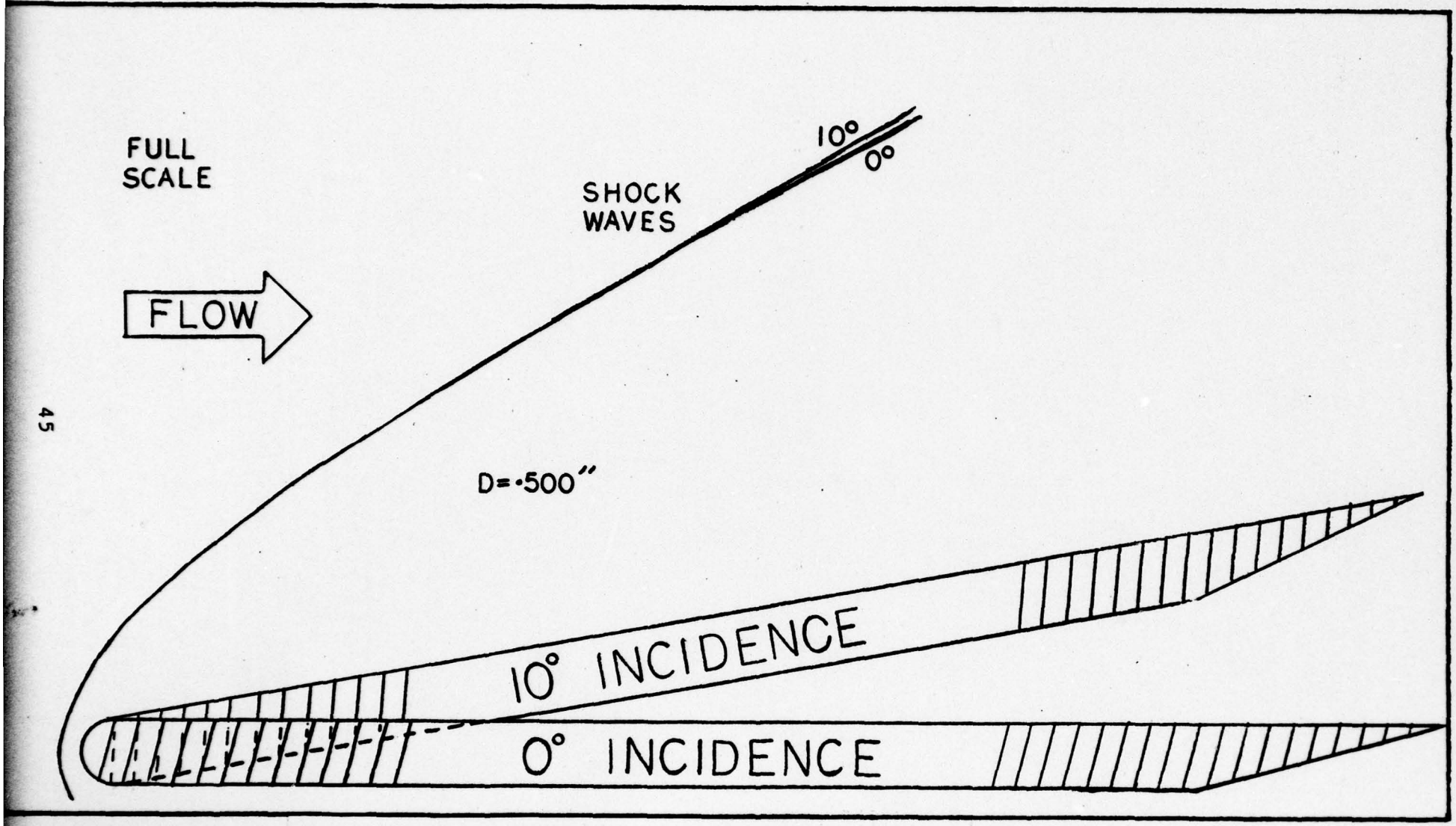

Figure 18. Effect of Incidence on the Observed Shock Wave Shape for D = 1.27cm (.500").

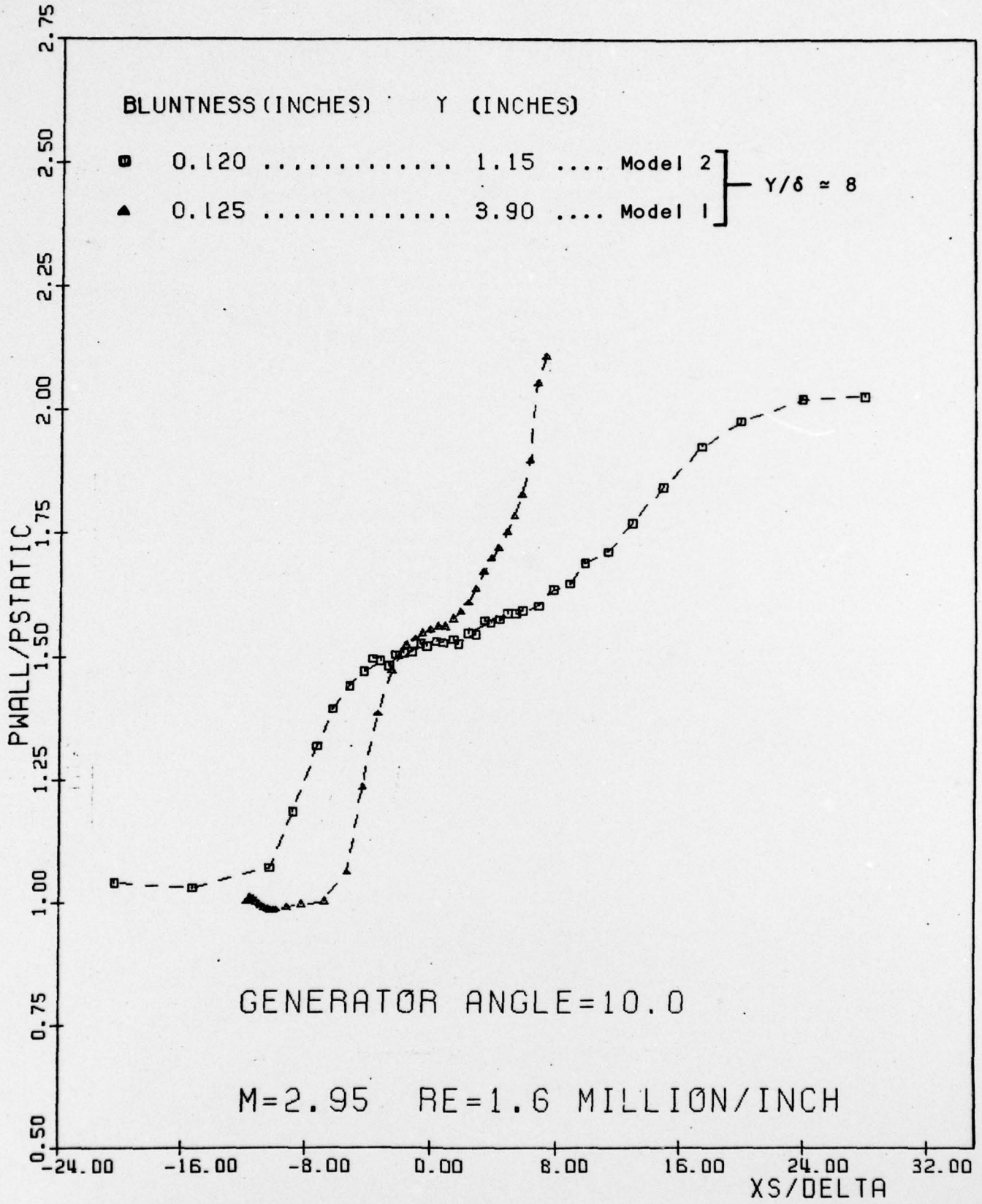

Figure 19. Measured Pressure Distributions as a Function of X_S/δ for a Given Y/δ — α_G = 10°.

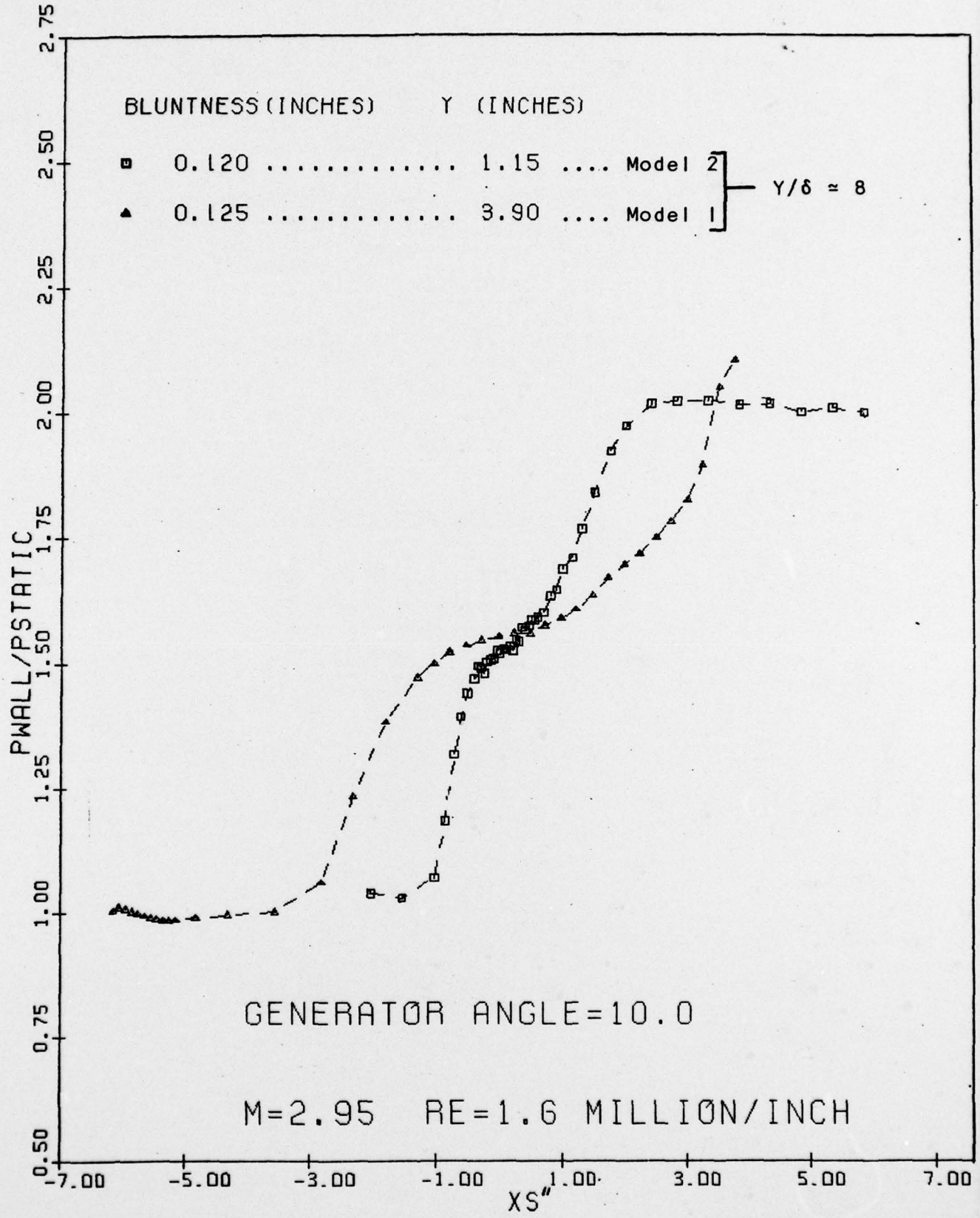

Figure 20. Measured Pressure Distributions as a Function of X_s for a Given Y/δ — α_G = 10°.

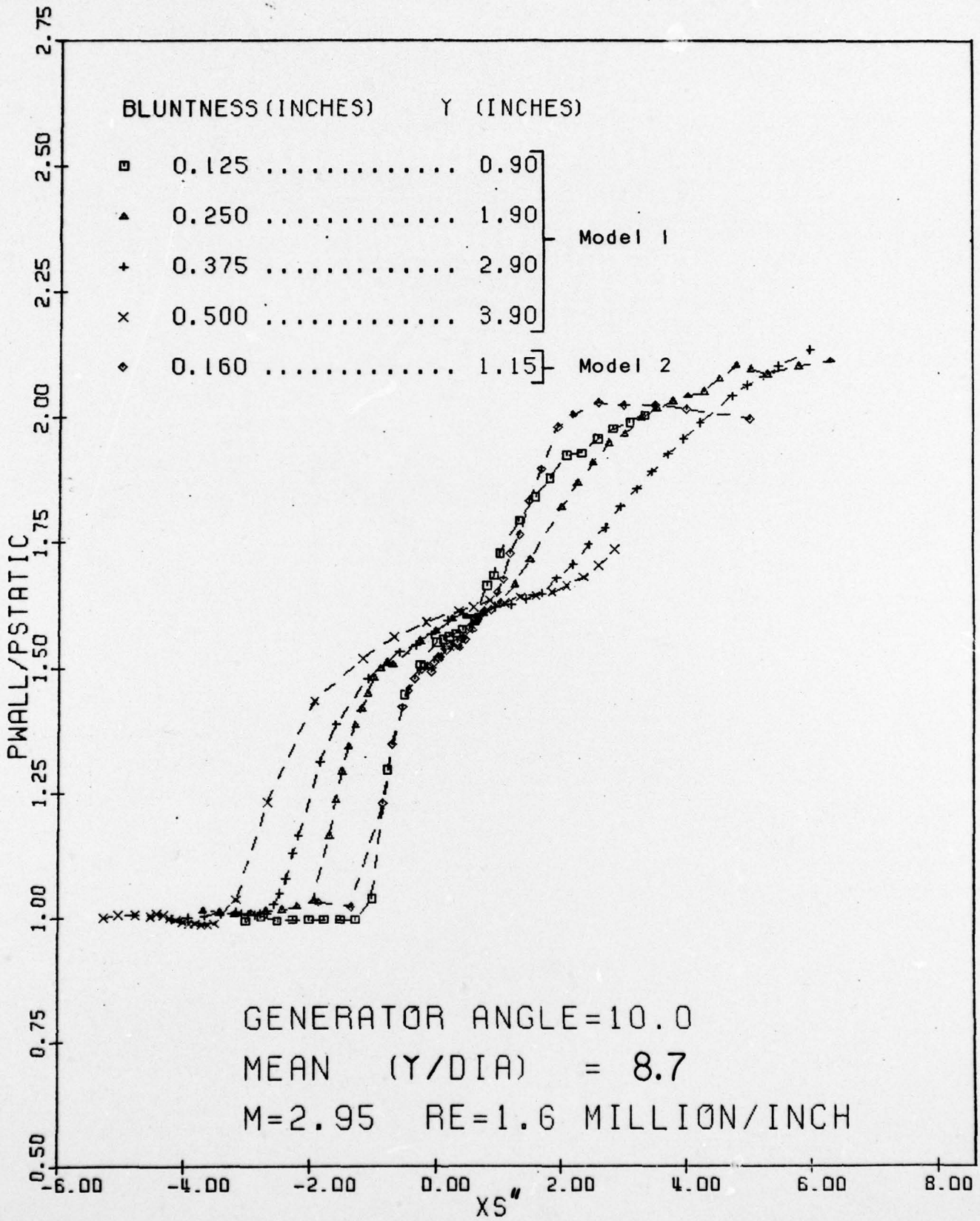

Figure 21. Measured Pressure Distributions as a Function of X_s for Y/D = 8.7 — α_G = 10°.

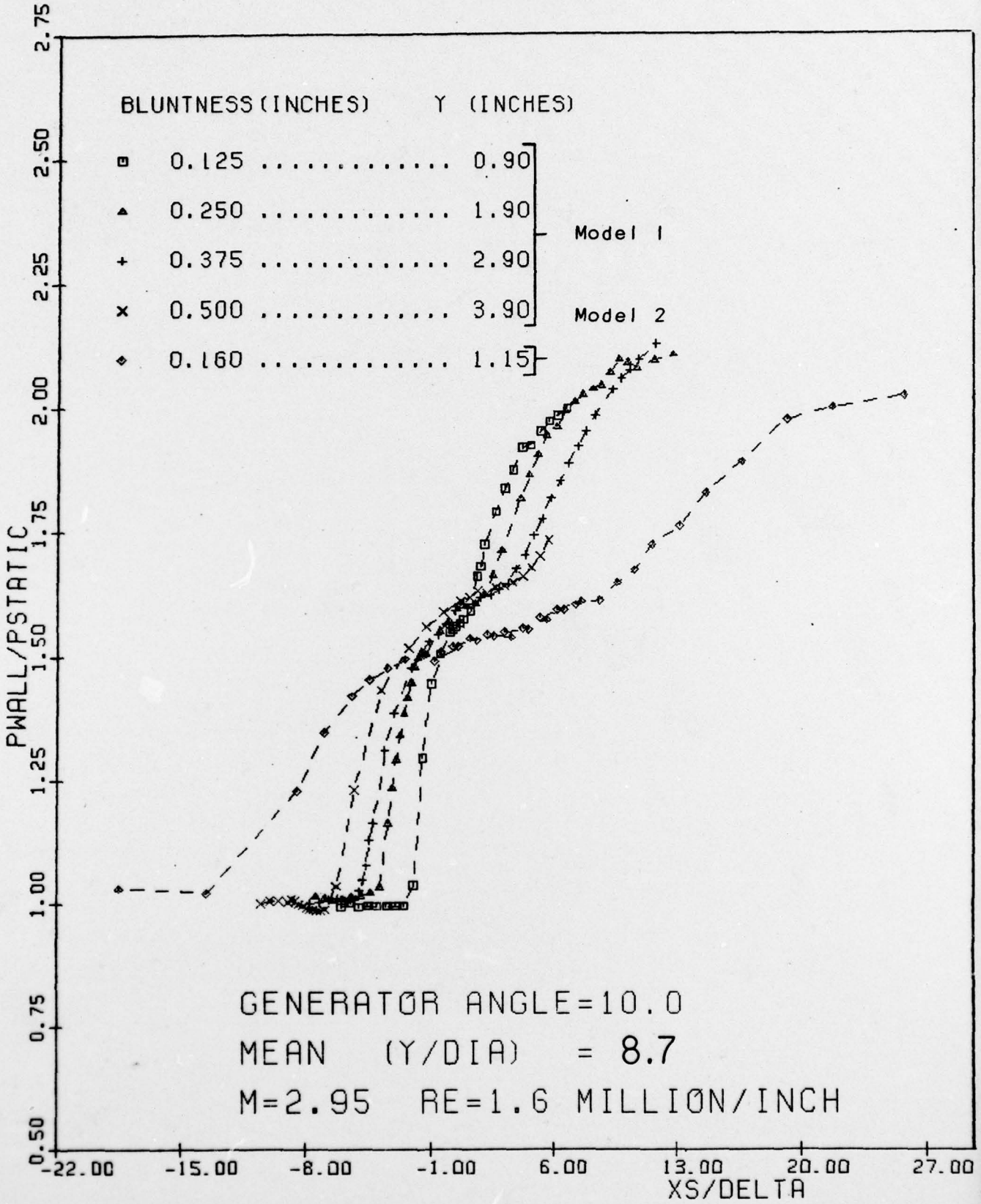

Figure 22. Measured Pressure Distributions as a Function of X_s/δ for Y/D = 8.7 — α_G = 10°.

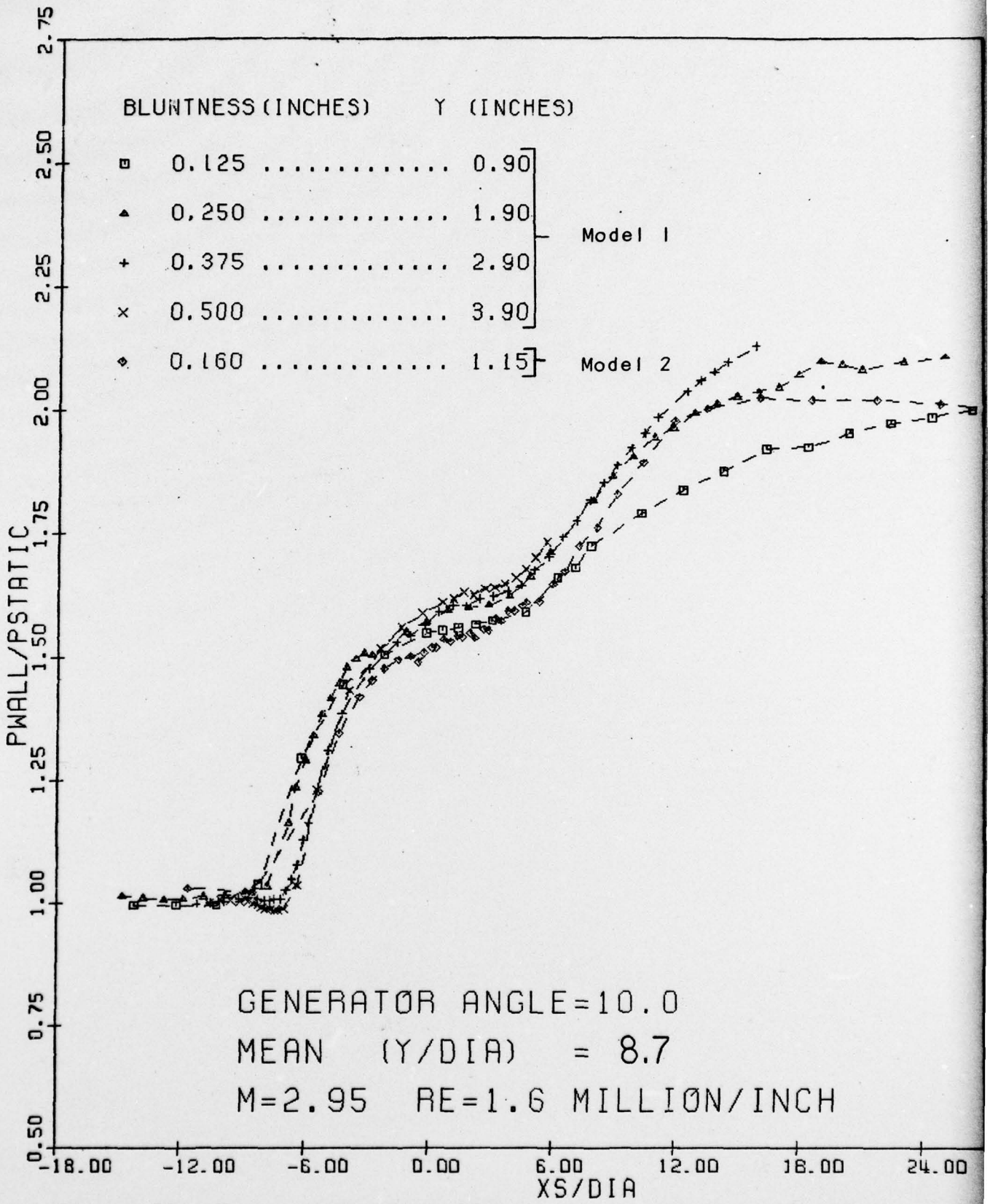

Figure 23. Measured Pressure Distributions as a Function of X_S/D for Y/D = 8.7 — α_G = 10°.

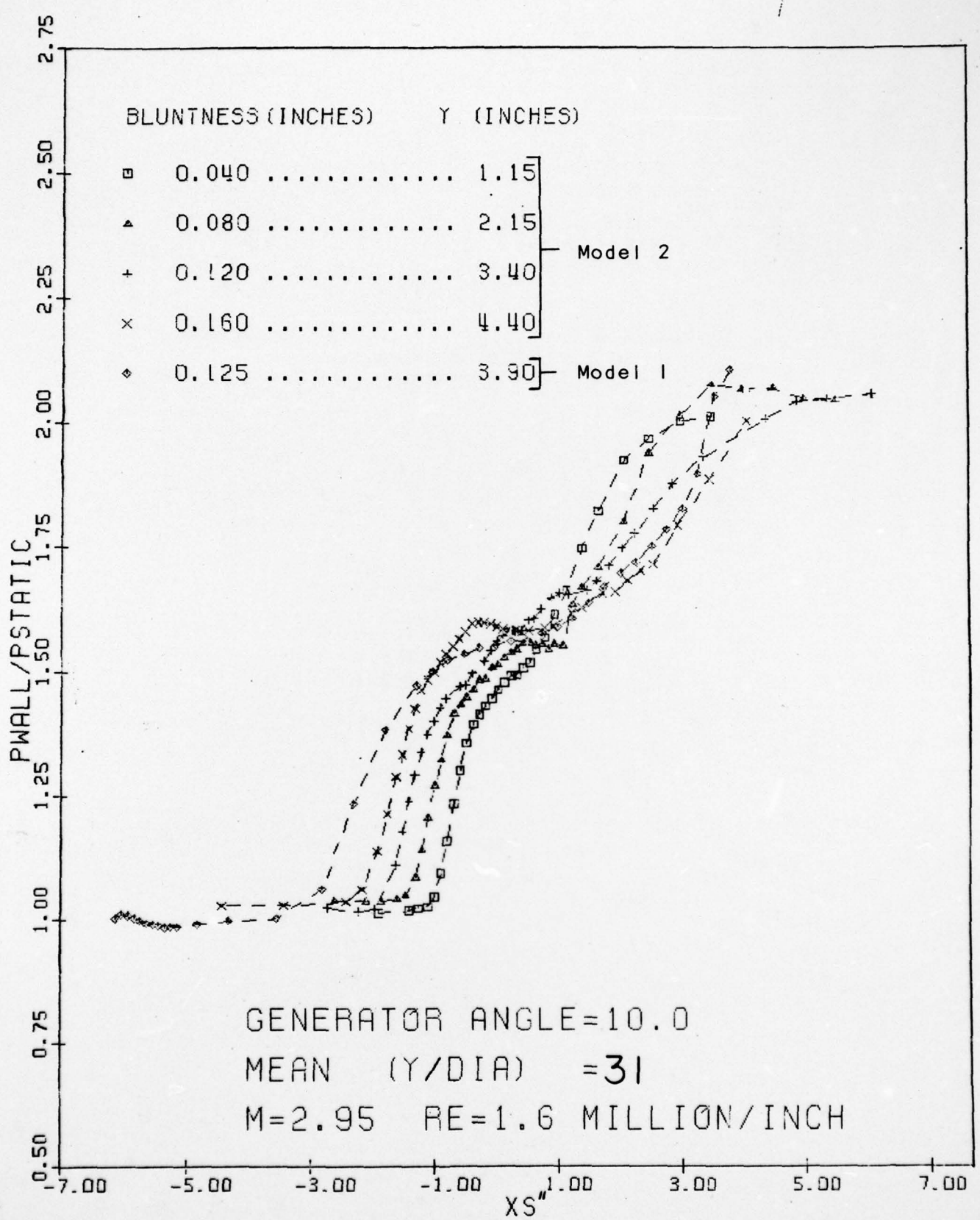

Figure 24. Measured Pressure Distributions as a Function of X_s for Y/D = 31 — α_G = 10°.

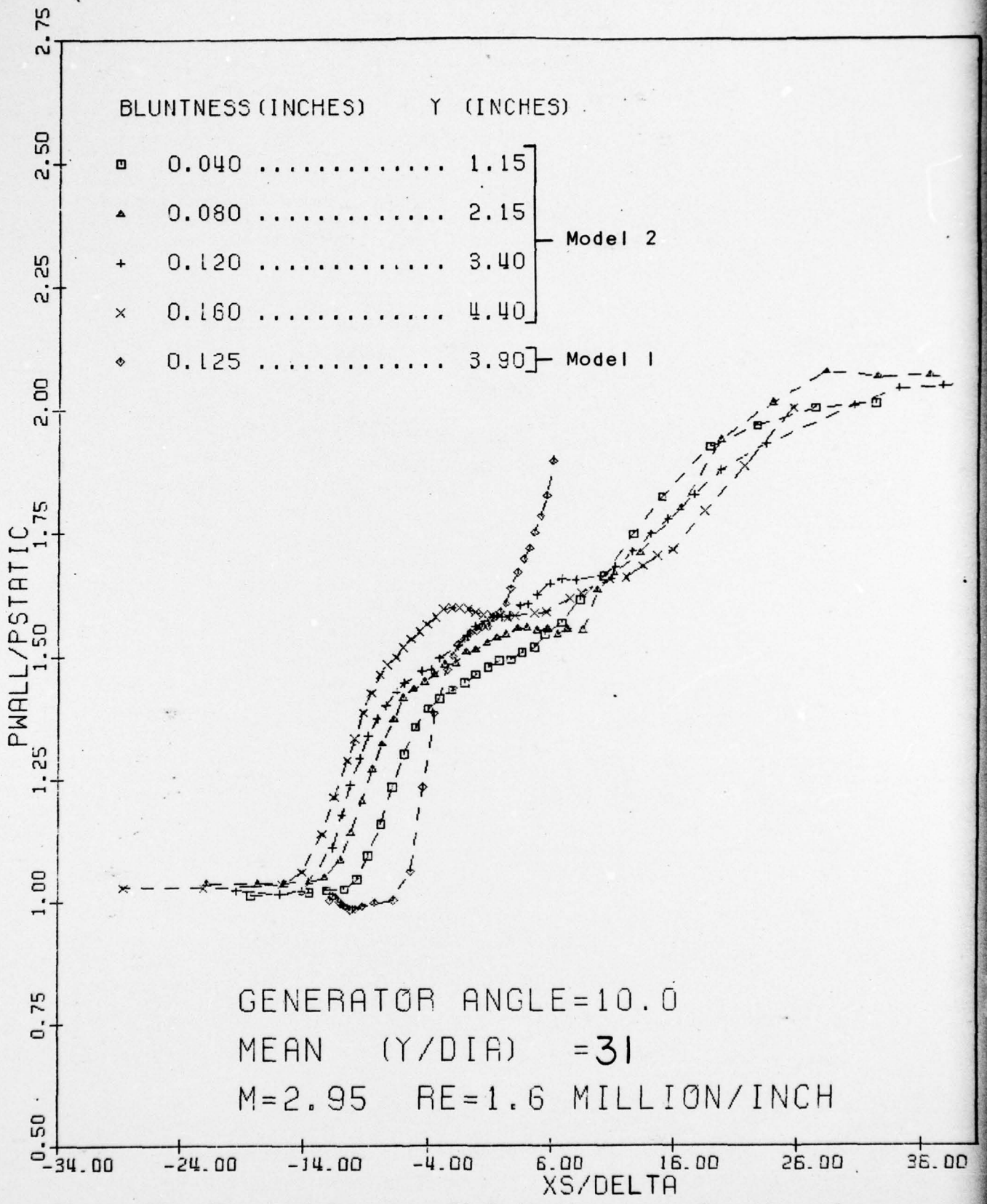

Figure 25. Measured Pressure Distributions as a Function of X_s/δ for Y/D = 31 — α_G = 10°.

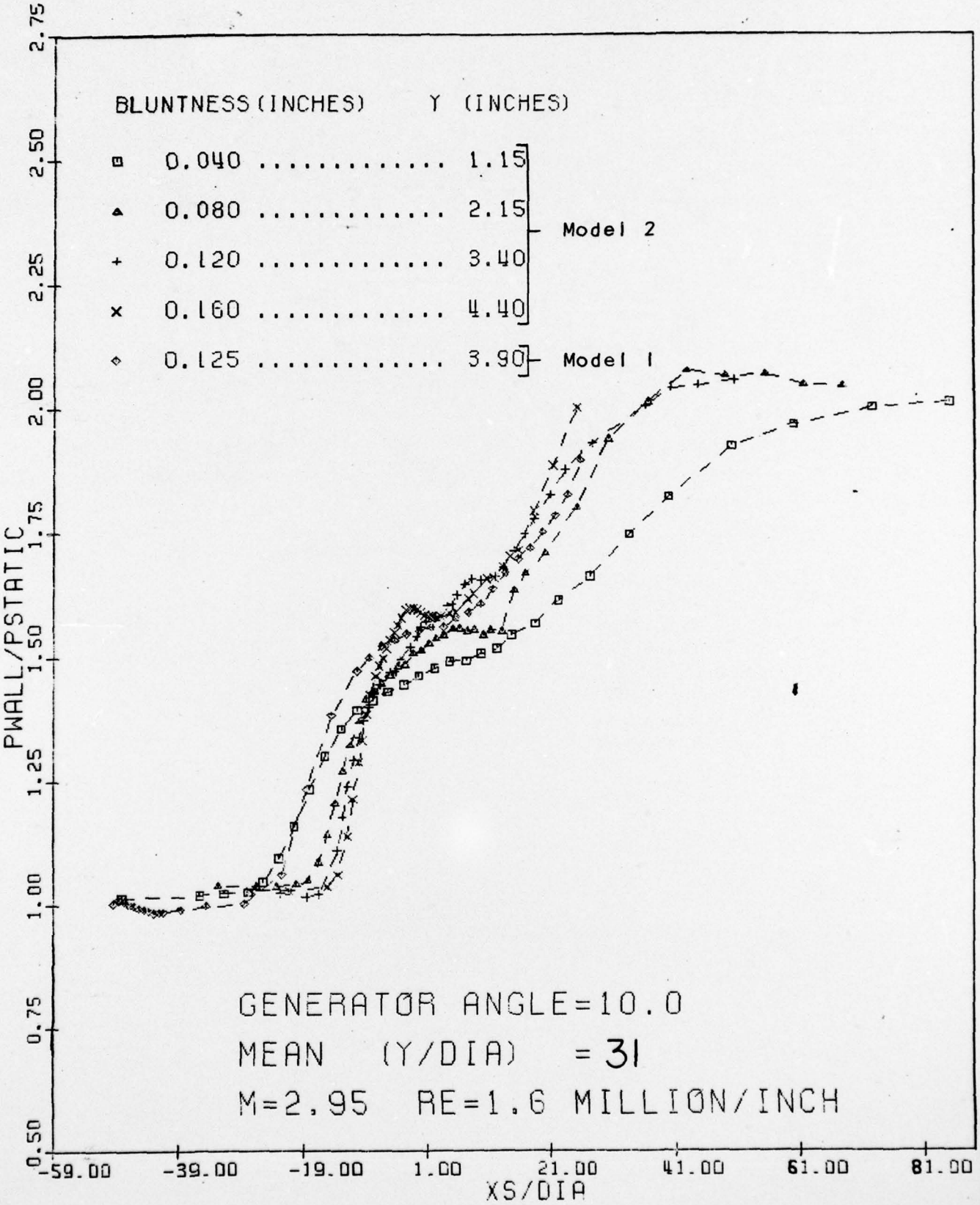

Figure 26. Measured Pressure Distributions as a Function of X_s/D for Y/D = 31 — α_G = 10°.

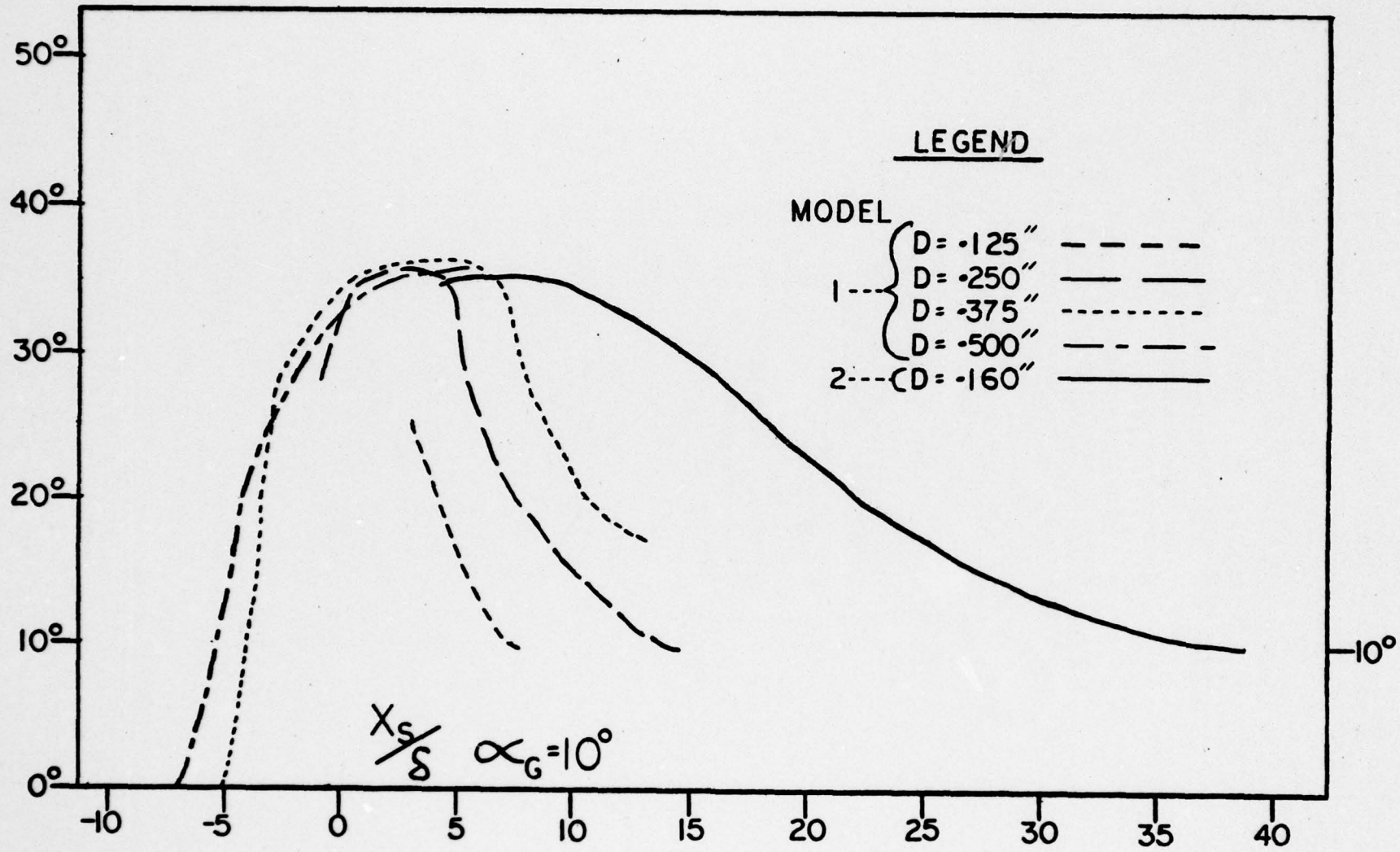

Figure 27. Surface Oil Flow Angles as a Function of X_s/δ for Y/D = 8.7.

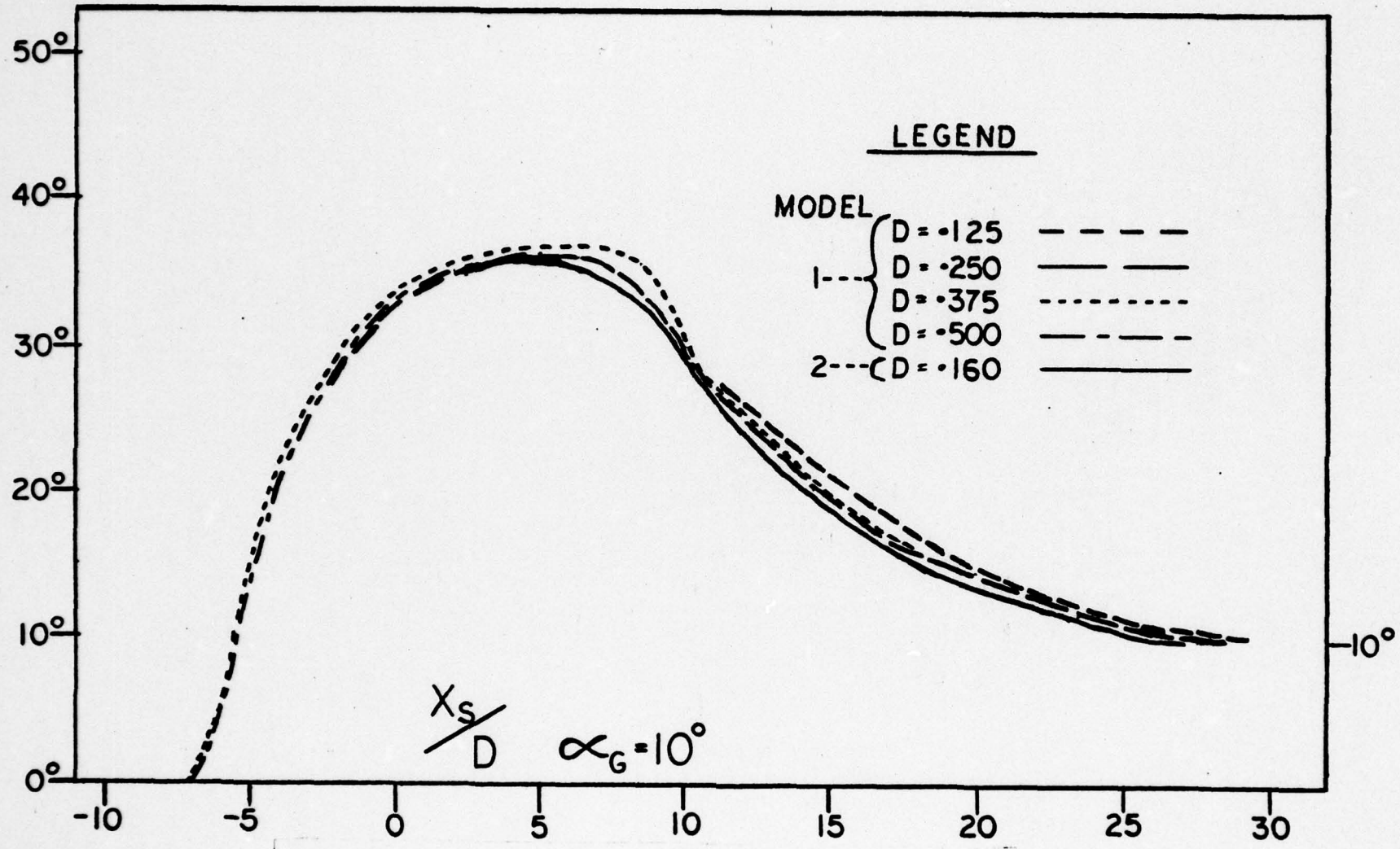

Figure 28. Surface Oil Flow Angles as a Function of X_s/D for Y/D = 8.7.

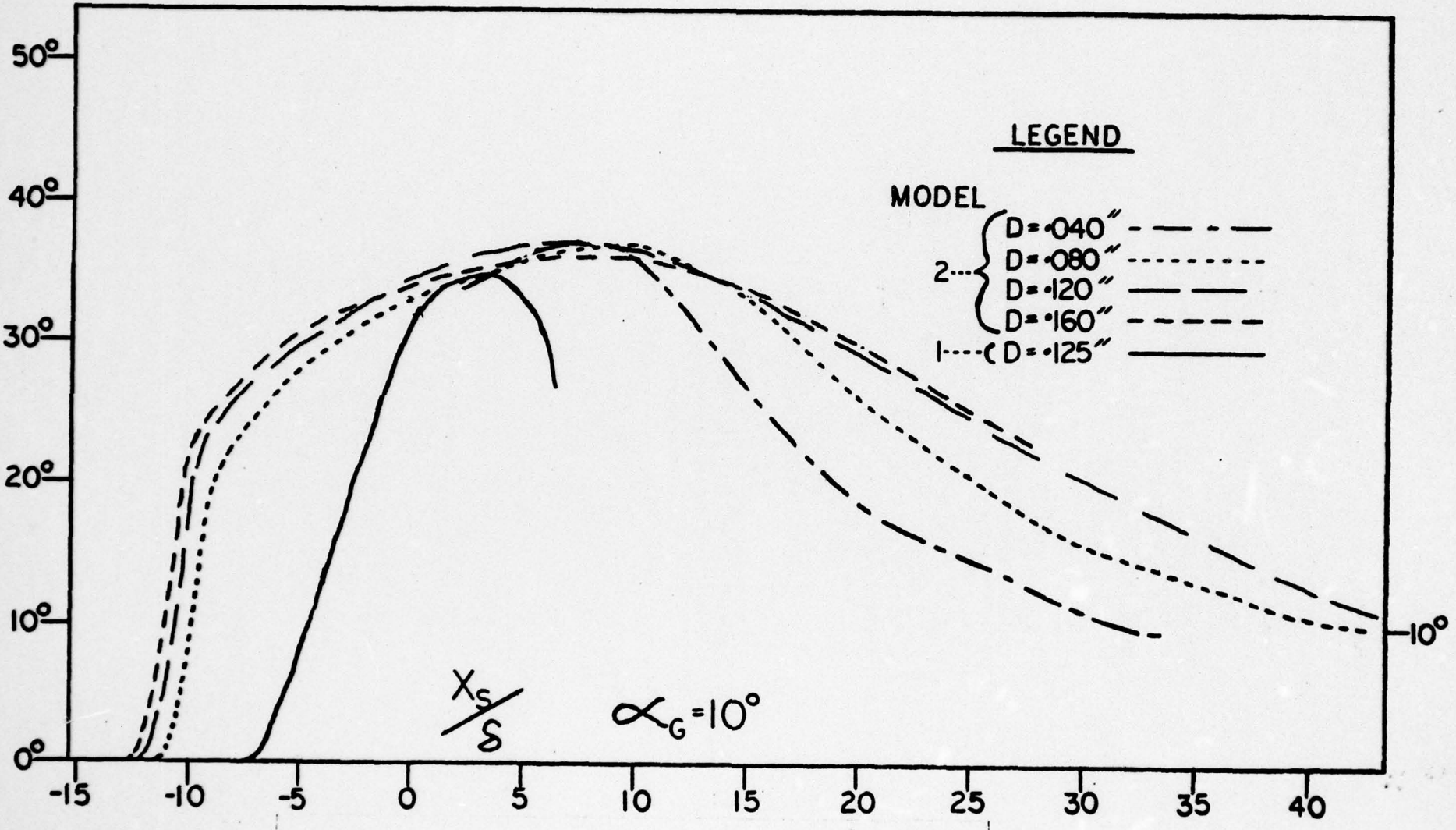

Figure 29. Surface Oil Flow Angles as a Function of X_s/δ for Y/D = 31.

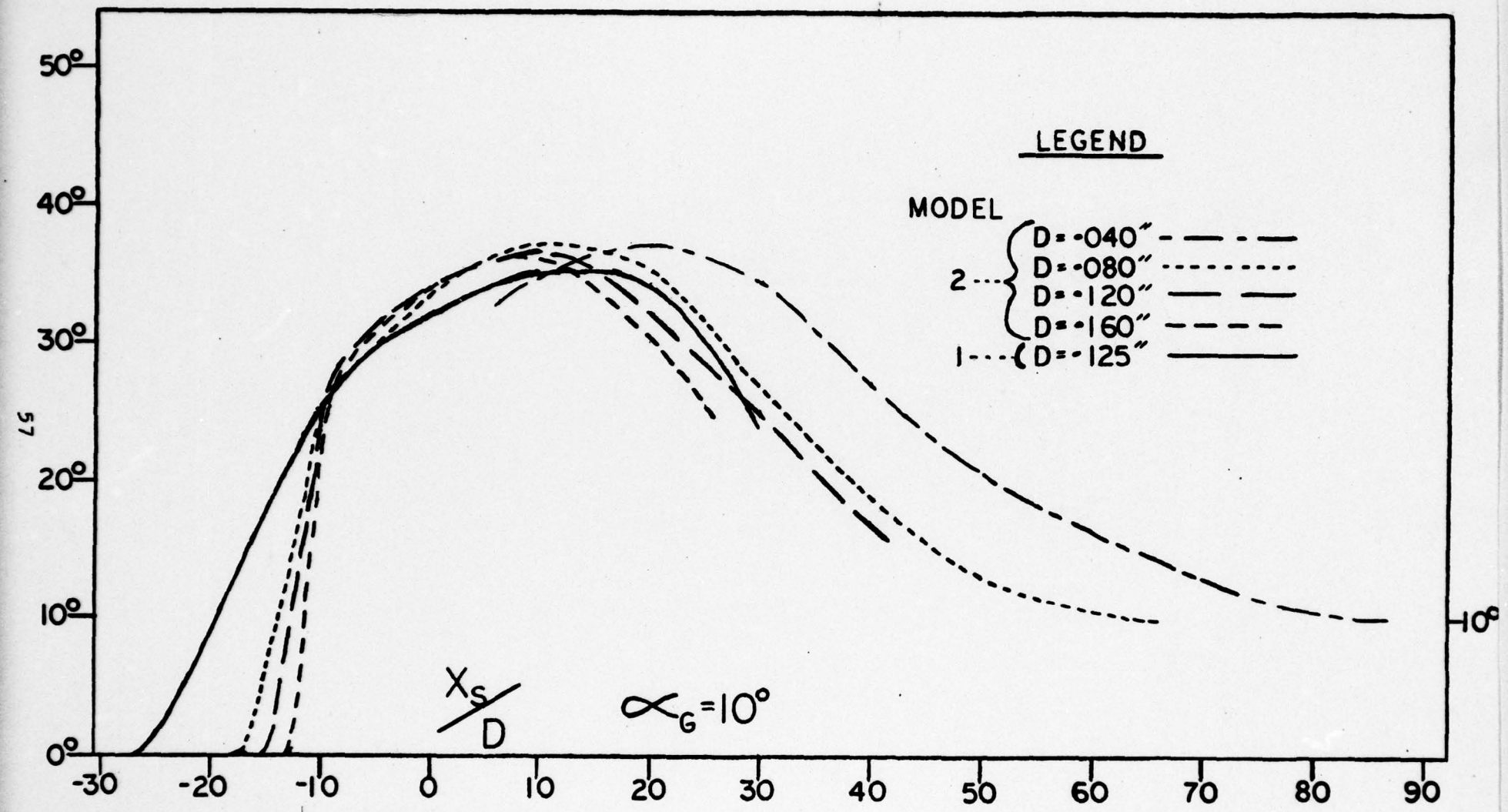

Figure 30. Surface Oil Flow Angles as a Function of X_s/D for Y/D = 31.

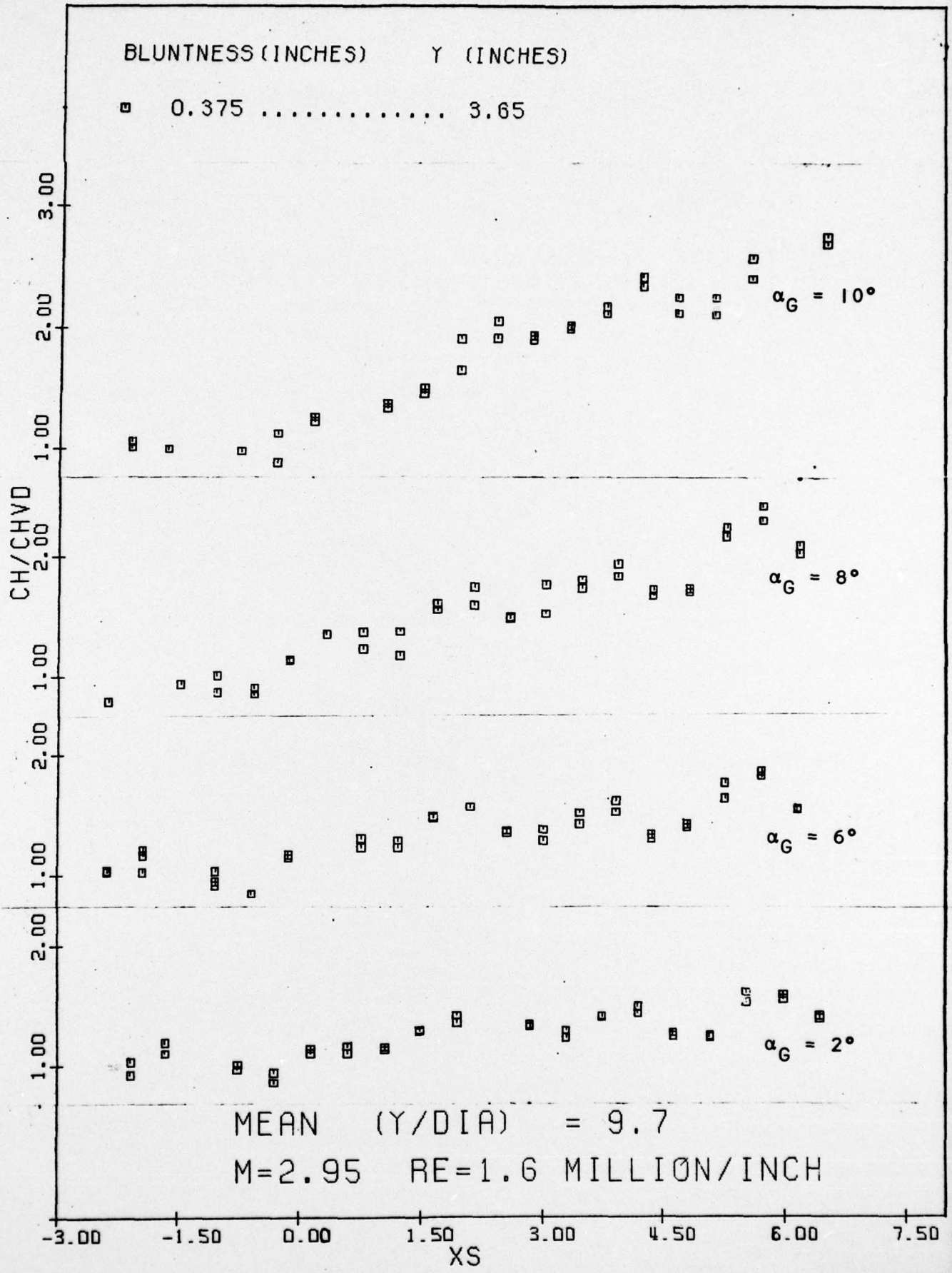

Figure 31 Effect of shock generator incidence on heat transfer coefficient distribution.

DISTRIBUTION LIST

Naval Air Systems Command (Code AIR-320C)
Department of the Navy
Washington, D. C. 20361
4 copies

Dr. Roland Lee (Code WA-41)
Naval Surface Weapons Center
White Oak Laboratory
Silver Spring, MD 20910
2 copies

Naval Surface Weapons Center
White Oak Laboratory
Silver Spring, MD 20910
Attn: Code WX-21
13 copies

ONR Resident Representative
Aero Laboratory, Forrestal Campus
Princeton University
Princeton, NJ 08540
1 copy